Materials Horizons

ROYAL SOCIETY OF CHEMISTRY

REVIEW

View Article Online
View Journal | View Issue

Cite this: *Mater. Horiz.*, 2025, **12**, 8261

Two-dimensional materials for adaptive functionalities in soft robotics

Yun Li,†[ab] Jiamin Amanda Ong †[ab] and Pooi See Lee *[ab]

Two-dimensional (2D) materials are critical for applications in tactile perception, health monitoring, virtual reality (VR), augmented reality (AR) and human–machine interfaces. In particular, recent advances in materials science, device fabrication, and machine learning have significantly propelled the applications of 2D materials for multifunctional soft robots owing to their flexible and conformal nature. In this review, we provide an overview of the fundamental mechanisms and recent breakthroughs in 2D materials for soft robotic systems, with a focus on their fabrication techniques, actuation mechanisms, and multiple sensing approaches. Subsequently, we highlight the significance of 2D materials in multimodal devices and feedback loop control for intelligent and smart robotics with self-adaptive manipulation. We then explore innovations such as multimodal sensing, human–robot interaction and artificial intelligence (AI)-promoted fast recognition. Finally, we summarize the future research directions and challenges, such as the reliable preparation roadmap for 2D materials and streamlined configuration to eradicate heavy wiring and enhance the dexterity of soft robots.

Received 29th March 2025,
Accepted 20th June 2025

DOI: 10.1039/d5mh00565e

rsc.li/materials-horizons

Wider impact

Flexible, multimodal, adaptive devices are pivotal to the integration of soft robots, offering a revolutionary approach to various bio-mimetic functions. Primary factors limiting the development of soft robotics include material preparation and device integration. The breakthroughs in two-dimensional (2D) materials have introduced new vitality in this field, allowing devices with higher performance without loss in their flexibility and conformability. This review explores the recent advances in 2D material-based actuators and sensors tailored for soft robotics, with a focus on their fabrication strategies, and their integration towards human–mimic motion and perception. Through an in-depth discussion on the advantages and disadvantages of each functional mechanism, a roadmap for further development of 2D material-based device integration is provided. This review not only summarizes the progress in this research field but also enriches the practical guidance for intelligent devices in soft robotics. These insights will help shape the next generation of 2D materials and devices, bridging the gap between materials science and advancing practical soft robots.

[a] *School of Materials Science and Engineering, Nanyang Technological University, 50 Nanyang Avenue, 639798, Singapore. E-mail: pslee@ntu.edu.sg*
[b] *Singapore-HUJ Alliance for Research and Enterprise, The Smart Grippers for Soft Robotics (SGSR) Programme, Campus for Research Excellence and Technological Enterprise (CREATE), 138602, Singapore*
† These authors contributed equally to this work.

Yun Li

Yun Li is currently a PhD candidate in the School of Materials Science and Engineering at Nanyang Technological University. His current research focuses on 2D material-based electronic devices and their applications in soft robotics.

Jiamin Amanda Ong

Jiamin Amanda Ong is currently a PhD candidate in the School of Materials Science and Engineering, Nanyang Technological University, where she received her bachelor's degree in 2019. Her research interests focus on the design and fabrication of halide perovskite-based piezoelectric sensors.

1. Introduction

Unlike traditional rigid and bulky robots, soft robots require flexible actuating parts and biomimetic sensors to deal with complex working conditions, such as intelligent grippers,[1] surgical operation,[2] and deep-sea exploration.[3] Fig. 1a illustrates the four core units and working principle of next-generation soft robots. The signals from the sensing part are analysed by the ''brain'' for making decisions. Thereafter, the commands from the ''brain'' are executed by a closed-loop controller by altering the electrical outputs to the actuator. The physical status of the actuator is adaptively controlled by this operation flow in real time. The dominant skeletons of the actuators and sensors in soft robots are usually soft materials, such as elastomers and hydrogels, considering their low Young's moduli and good mechanical stability.[4,5] However, only soft materials cannot provide sufficient or satisfactory functionalities, such as adequate actuation efficacy and human–mimic perceptions (sight, taste, smell, sound and tactile). A selective functional stimuli-responsive filler or responsive active layer in the device is indispensable to enable intelligent soft robotics.

The recent advances in two-dimensional (2D) materials, originating from graphene,[6] have accelerated development in various fields owing to their unique physical and mechanical properties, such as high conductivity, large surface area, good flexibility, excellent mechanical strength and tunable electrical structures. Benefiting from these properties, flexible electronic devices, actuators and sensors in particular, have been greatly developed.[7–11] With the exploration of material properties and device integration, these devices have offered various potentials to soft robotics. Despite the revolutionary development of 2D materials and their abilities to create an intelligent soft robot system, several critical technological challenges need to be addressed. The technological limitations arise primarily from the mismatch between the mechanical properties of 2D materials and the soft substrates/matrix, as well as the poor compatibility between the preparation process of the 2D materials and the soft substrates/matrices. There are some technological and design breakthroughs that have provided solutions to these problems, such as 2D material–polymer composites,[12,13] low-temperature fabrication of 2D materials[8,14] and device encapsulation.[15–17] Moreover, the recent strides in multimodal device and closed-loop feedback control enable a more complete intelligent soft robot system.[18–20]

In this review, we focus on the representative works on 2D materials that potentially serve as actuators and sensors in soft robotics. First, we discuss the importance of 2D materials in soft robotics applications, by comparing different fabrication techniques of 2D materials and highlighting the most suitable fabrication techniques for different requirements. At the actuator frontier, an overview of the various actuation mechanisms and motion types based on 2D materials is provided. At the sensor frontier, we categorize the sensors by five representative human–mimic perceptions (sight, taste, smell, sound and tactile), alongside multimodal sensing and the integration attempts towards artificial intelligence (AI) and human–machine interface (HMI). Importantly, we highlight the current limitations of integrating 2D materials into soft robots, and the possible solutions. These challenges include low-temperature integration, device integration (multiple functions in one device instead of device arrays) and adaptive control.

Pooi See Lee

Pooi See Lee is the President's Chair Professor of Materials Science and Engineering at Nanyang Technological University (NTU), Singapore. Her current research focuses on developing stretchable elastomeric composites for electronics and energy devices, human–machine interfaces, sensors and actuators, and hybrid materials for soft robotics. Prof. Lee was elected the Fellow, National Academy of Inventors in 2020, Materials Research Society Fellow in 2022, and she is a Fellow of the Royal Society of Chemistry.

2. Advantages of 2D materials in soft robotics

From the advent of graphene,[6] various 2D materials have been extensively explored and investigated, including transition-metal dichalcogenides (TMDs), hexagonal boron nitride (h-BN), Xenes, MXenes, transition-metal oxides (TMOs), and 2D perovskites.[21] Fig. 1b illustrates the deployment of various 2D materials across specific applications within the soft robotics domain, highlighting that graphene continues to dominate research efforts in this area. The integration of 2D materials into soft robotics has revolutionized the field, enabling systems with unprecedented flexibility, sensitivity and multifunctionality.

2.1 Flexibility and conformability

Flexible materials with light and compliant characteristics are essential for the integration of soft robotics. Two-dimensional materials are particularly promising for this application owing to their ultrathin thickness (down to 1 nm), mechanical flexibility, and light weight. This allows seamless integration into deformable structures. Young's modulus (E) and strain limit are the two key parameters to evaluate the served devices in soft robotic systems.[21] Fig. 2a and b show Young's moduli and the strain limit of different 2D materials. The mechanical flexibility of 2D materials is defined by stiffness (K) with a relation of $K = E \times \frac{A}{L}$, where A and L are the cross-sectional area and the length of the material. The ultralow cross-sectional area of atomically thin 2D materials offers a very low stiffness,[22]

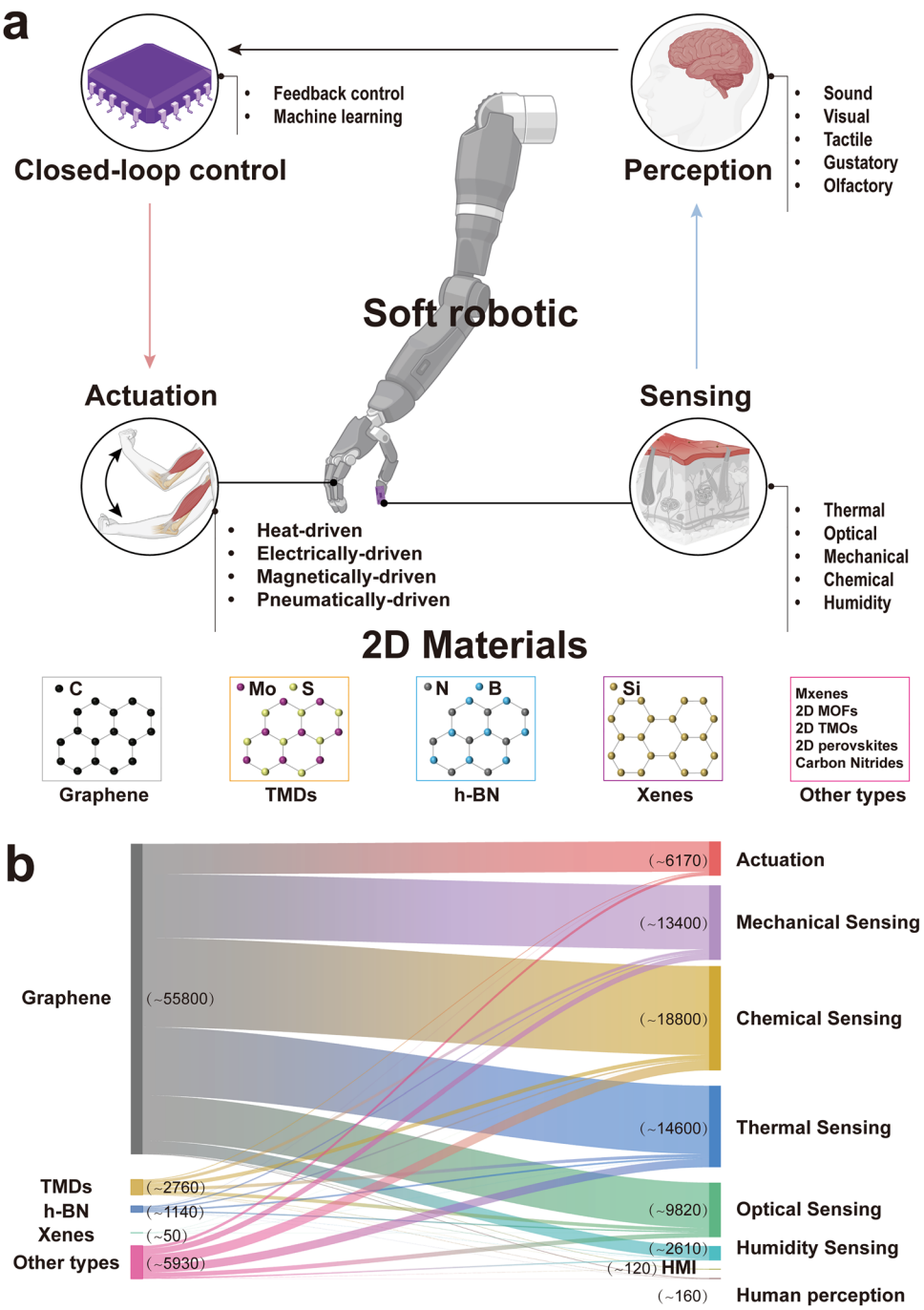

Fig. 1 Overview of 2D materials for soft robotics with a focus on the actuation and sensing directions. (a) Soft robotic and its four core units: actuation, sensing, perception (decision-maker) and control part. Created using BioRender: https://BioRender.com. (b) Sankey diagram visualizing the use of different 2D materials with various applications. Each vertical bar represents the number of publications per field. Data: Web of Science till the end of January 2025.

thereby showing decent flexibility in nature. The strong intra-layer covalent bonding in layered 2D materials provides them with high in-plane mechanical strength and high strain limit. The synergistic effect of both low thickness and strong intra-layer covalent bonding in 2D materials makes them suitable for soft robotics. It should be noted that Young's modulus of each 2D material is slightly increasing with the lower thickness due to the lower presence of stacking faults in a thinner film.[23] For example, Young's modulus for an ultrathin MoS_2 flake is around 0.27 TPa, while the value for bulk MoS_2 is around 0.24 TPa.[24] Graphene shows higher Young's modulus (~1 TPa) among most other types of 2D materials, but also a higher strain limit (~25%), enabling it to withstand large strain during service (Fig. 2b).[25] Moreover, 2D materials with large

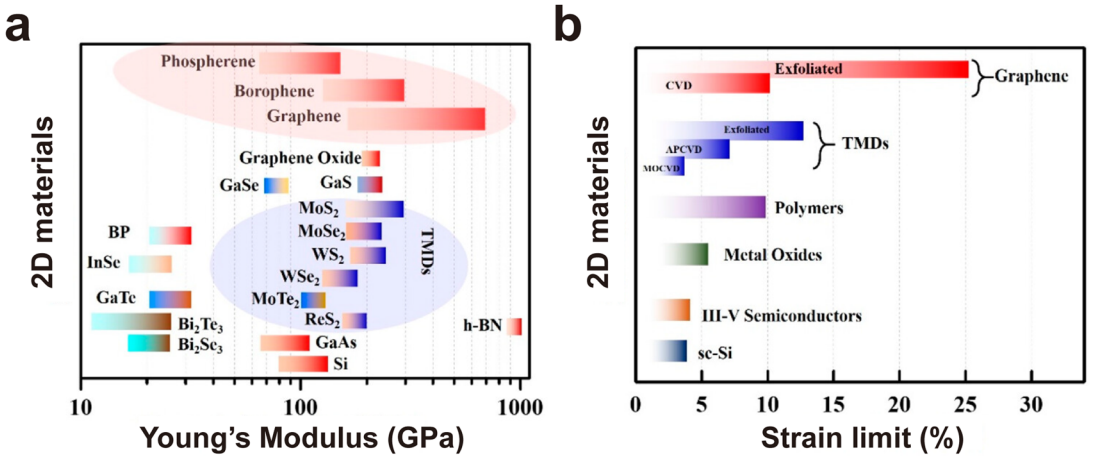

Fig. 2 Mechanical properties of 2D materials: (a) Young's modulus. (b) Fracture strain limit. Reproduced with permission.[21] Copyright 2024, American Chemical Society.

area are preferred in soft robotics due to the high flexibility in large-scale sheets or films according to the equation of $K = E \times \frac{A}{L}$.

Therefore, the first advantage of 2D materials in soft robotics is their flexibility, which however poses a challenge to the fabrication process. The thinner and larger the 2D materials, the better their performance. However, a freestanding larger 2D film of centimetre scale is too fragile to work with dynamic robots. Due to their intrinsic mechanical properties and ultrathin nature, the freestanding large 2D films without any substrate support have limited capacity to distribute and absorb mechanical stresses, making them susceptible to deformation and fracture.[26] Integrating them onto flexible substrates such as elastomers or hydrogels is a good option. The second demand for this application is conformability and self-adhesion to these soft substrates. Due to the low bending stiffness and high strain limit of 2D materials, this second requirement is met, providing good conformal contact ability. This underlines the near-perfect contact interface between 2D materials and support substrates, such as the 2D electronic tattoos on polyimide (PI)[27] or tattoo paper,[28] enabling a high signal-to-noise ratio during operation.[25] The extremely thin characteristics will not affect the deformation and rebound of the bottom support polymer, and hence, the entire device has good motion deformation ability.

2.2 Sensitivity to stimuli

The large surface-to-volume ratio of 2D materials enhances their sensitivity to external stimuli. For instance, transition metal dichalcogenides (TMDs) like MoS_2 have been used in strain sensors with ultrafast response times (<10 ms) and high gauge factors (>100), critical for detecting subtle deformations in soft grippers.[29] For smell and taste perception in soft robotics, molecules are tending to be adsorbed and differentiated by 2D materials due to the abundant exposure of the active sites on 2D materials.[21] Furthermore, the in-plane charge flow promotes a fast response to stimuli due to the ultrathin nature.

Besides, the large surface-to-volume ratio of 2D materials enables efficient light–matter interactions, allowing higher photocurrent in optoelectronic devices. A single-layer MoS_2-based flexible photodetector showed tunable photoresponsivity (by 2–3 orders of magnitude) and response time (as fast as 80 ms). The adjustable performance can be attributed to modified strain in MoS_2 films.[30] For thermal and photothermal applications, 2D materials have attracted more attention due to their excellent thermal conductivity and significant photothermal effects.[31,32] For example, $Ti_3C_2T_x$ can be integrated into a thermal indicator from 20 to 160 °C due to its high photothermal conversion efficiency.[33]

Hence, the atomic thickness, outstanding electrical and thermal conductivity as well as the extensive surface-to-volume ratio of 2D materials confer exceptional sensitivity and rapid responsiveness to various stimuli (including strain, molecular interactions, light, and thermal changes), making them highly promising for applications in soft robotics, particularly in sensing components.

2.3 Layer-dependent and phase-dependent electrical and optical properties

Two-dimensional materials include those exhibiting metal, insulator or semiconductor properties with adjustable bandgaps.[21] The diverse electrical and optical properties of 2D materials, influenced by the number of layers, composition, and the defect density in 2D materials, offer a wide selection range for advanced devices in soft robotics.[6,34] For example, monolayer graphene with a zero bandgap can change to a small bandgap for the bilayer state. MoS_2 shows a direct bandgap ($\sim$1.8 eV) for monolayer form but an indirect bandgap ($\sim$1.2 eV) in bulk.[34] In addition to the thickness, different phases of each 2D material also feature distinct electrical and optical properties. MoS_2 encompasses metallic phase (1T), semiconducting phase (2H) and metal stable ferroelectric

phase (3R).[35,36] The synergy between thickness effect and phase effect is critical to optimize the properties of 2D materials, opening a window for diverse device integration.

2.4 Stability

Apart from the attractive flexibility and conformability, as well as the sensitivity to multiple stimuli, other physical properties, especially stability in 2D materials, deserve more attention. Material stability, including thermal stability, photostability, and ambient stability, is vital to achieve long-term durability for integrated devices. Thermal stability is important for materials used in environments with varying temperatures. Among 2D materials, h-BN exhibits exceptional thermal stability. Monolayer h-BN remains stable up to 850 °C in air,[37] outperforming graphene, which starts oxidizing at 250 °C and is etched at 450 °C.[38] Interestingly, the defect density, number of layer of 2D materials and the interface interaction between the substrates and 2D materials also contribute to the thermal stability. For example, the thermal stability of single-layer MoS_2 is better than that of few-layer MoS_2 on Al_2O_3 or SiO_2 substrates, while it is worse than that of few-layer MoS_2 on mica.[39] Photostability refers to a material's resistance to degradation upon exposure to light, a crucial factor for materials in optoelectronic applications, which is highly dependent on the composition of 2D materials. For instance, monolayer MoS_2 (stable for 4 hours under continuous photoirradiation of 580 nm, 800 W cm^{-2}) exhibits higher photostability than monolayer WS_2 (degradation from 90 min under an identical photoirradiation condition).[40] Black phosphorus (BP), while exhibiting high carrier mobility, suffers from rapid degradation upon exposure to air, leading to compromised electrical properties. This air sensitivity poses challenges for its direct application under ambient conditions.[41] Similarly, the severe oxidative degradation of MXenes compromises their structural integrity and electrical conductivity, limiting their practical applications. This degradation is influenced by various factors, including the quality of the parent MAX phase, chemical etching conditions during synthesis, and storage environments.[42] M. van Druenen reviewed the strategies to enhance the ambient lifetime of BP,[41] while Iqbal *et al.* introduced the solutions to improve the oxidation stability of 2D MXenes.[42] The 2D perovskites, unlike other 2D materials, show poorer stability with lower dimensions, but superior stability to their 3D counterparts. This arises from their unique molecular architecture (large organic cation spacers sandwiched by octahedral layers), which imparts resistance to environmental factors such as moisture and oxygen, making them promising materials in optoelectronic applications.[43]

Understanding the stability profiles of 2D materials is critical for their successful application in soft robotics. Materials such as h-BN and MoS_2 offer promising stability, making them suitable for integration into flexible actuators and sensors. Specifically, the exceptional thermal stability and chemical inertness make h-BN an ideal candidate for insulating layers in flexible electronic components, protecting sensitive elements from thermal and oxidative damage. MoS_2 can serve as a suitable material for photodetectors and transistors in soft robotic systems due to its robustness under ambient conditions and relative photostability. In contrast, materials with inherent environmental sensitivities necessitate protective measures to enhance their viability. Ongoing research into stabilization techniques, encapsulation procedures, and a deeper comprehension of degradation mechanisms will further expand the potential of 2D materials in the realm of soft robotics.

2.5 Fabrication and integration strategies of 2D materials into soft robotics

Table 1 compares the representative fabrication techniques for 2D materials. These fabrication techniques can be broadly classified into two primary methods: top-down and bottom-up. Top-down methods aim to produce 2D flakes by breaking down the bulk crystals, while bottom-up approaches produce 2D material films *via* various precursors. Katiyar *et al.* reviewed the recent advances of different fabrication methods for 2D materials.[21] The fabrication process of 2D materials significantly affects the material properties such as defect density and thickness uniformity, which, in turn, determine the device performance. To integrate into soft robotics, large-area devices based on 2D materials can be prepared by two strategies: (1) devices made by solution-based processing; (2) devices made by deposition methods.

Devices made by solution-based processing involve the preparation of 2D flake solutions (2D inks), followed by dispensing inks on desired substrates using printing or casting (such as inkjet printing, screen printing, drop-casting, spin coating and spray coating). This strategy is compatible with soft robotics due to their reduced cost and scalability. However, flake or layer aggregation is the primary challenge to limit the development of this method. The concentration and rheological properties of 2D inks must be adjustable for compatibility with different deposition techniques. Otherwise, film defects will significantly decrease the device performance. For example, suitable rheology and concentration of inks are always required to prevent flake aggregation, solvent evaporation, and nozzle clogging.[44] To enable their use in soft robotic applications, 2D inks are often mixed with a polymeric network to achieve enhance network cohesion and substrate adhesion. Chemical coupling is often used to compatibilize the functionalized 2D inks with the polymer matrix. Pinilla *et al.* reviewed the main scientific and technical limitations currently faced by 2D inks and the related printing technologies.[45] The optimization of the 2D ink formulation is the key to fabricate devices using solution-based approaches.

Although deposition techniques provide reliable quality and controllable thickness of 2D material films, their high thermal budget and often the need of vacuum is incompatible with the polymeric substrate/matrix that are needed for soft robotics. For example, polydimethylsiloxane (PDMS) and Ecoflex are the widely used elastomers for stretchable devices, while PET and PI are the most popular substrates/matrices for bendable devices with operation temperatures below 300 °C.[46–49] Hence, temperature is the primary factor determining the selection of

Table 1 Summary of representative fabrication techniques for 2D materials

Method	Temperature	Advantages	Disadvantages	Application	Ref.
Mechanical exfoliation	Room temperature	Simple, high-quality monolayers, minimal defects	Low yield, small flake size, non-scalable	Graphene, TMDs, Xenes	56
Sputtering	<50 °C	Large-area deposition, good uniformity, compatible with industrial processes	High defect density, limited to specific materials	Oxides, nitrides, carbides	57
Thermal evaporation	<100 °C	High-purity films, good thickness control	Poor adhesion, limited to low-melting-point materials	Metals, conductors	58
Composite	<150 °C	Scalable, flexible substrates, low thermal budget, roll-to-roll compatible	Poor flake alignment, agglomeration, low conductivity	Graphene, h-BN, TMDs, MXenes	44
ALD	50–300 °C	Atomic-level thickness control, excellent conformality, low defect density	Extremely slow, limited material selection	h-BN, TMDs, TMOs	59
Thermal decomposition	300–400 °C	Low-cost, solution-processable, flexible substrate compatibility	Non-uniform layers, residual impurities, limited crystallinity	Oxides, TMDs	51
Low-thermal-budget CVD	300–500 °C	BEOL-compatible (<400 °C), direct growth on CMOS/flexible substrates, high uniformity	Requires precursor engineering, reactor design complexity	TMDs	8
MOCVD	500–800 °C	Precise layer control, doping compatibility, scalable	Expensive precursors, toxic byproducts, complex setup	Graphene, h-BN, TMDs,	60
Conventional CVD	600–900 °C	High crystallinity, large-area growth, versatile for various 2D materials	High energy cost, substrate limitations, slow cooling required	Graphene, h-BN, TMDs,	60

integration techniques for soft robotic applications. With the intensive studies on the fabrication techniques for 2D materials, from mechanical exfoliation to physical vapor deposition (PVD) to chemical vapor deposition (CVD), the methods can be categorized to two types: direct growth and indirect transfer. Fig. 3 illustrates the processing temperatures for different fabrication methods. At the growth frontier, the processing temperature varies from ~100 °C for PVD (including sputtering and thermal evaporation) to 600–900 °C for CVD.[50–52] The PVD process provides high uniformity at a wafer scale with low thermal budget, but introduces high defect density, lowering the device performance. The primary defects are grain boundaries and vacancies, which often need post-treatment to mitigate, thereby enhancing thermal budget (*e.g.*, mitigate oxygen vacancies by annealing in an oxygen atmosphere at high temperatures). The high processing temperature for CVD makes it a non-preferable method to integrate a soft device although it is more reliable to control the thickness and crystallinity on a large scale among other direct growth methods. To use the high-quality deposited 2D films by CVD, an indirect transfer process is widely used.[53] For example, CVD-grown TMDs are widely integrated into field-effect transistors by wet-transfer or dry-transfer processes.[52] However, devices made with transfer processes tend to suffer from four main challenges: mechanical damage, contamination, scalability and high variability in performance. Cheliotis *et al.* reviewed the transfer techniques of 2D materials.[54] Therefore, devices made by transfer process are compatible with soft robotic applications but achieving near-clean transfer with large area is inevitable.

To overcome the high thermal budget in the CVD process, low thermal budget CVD (low-T CVD) and atomic layer

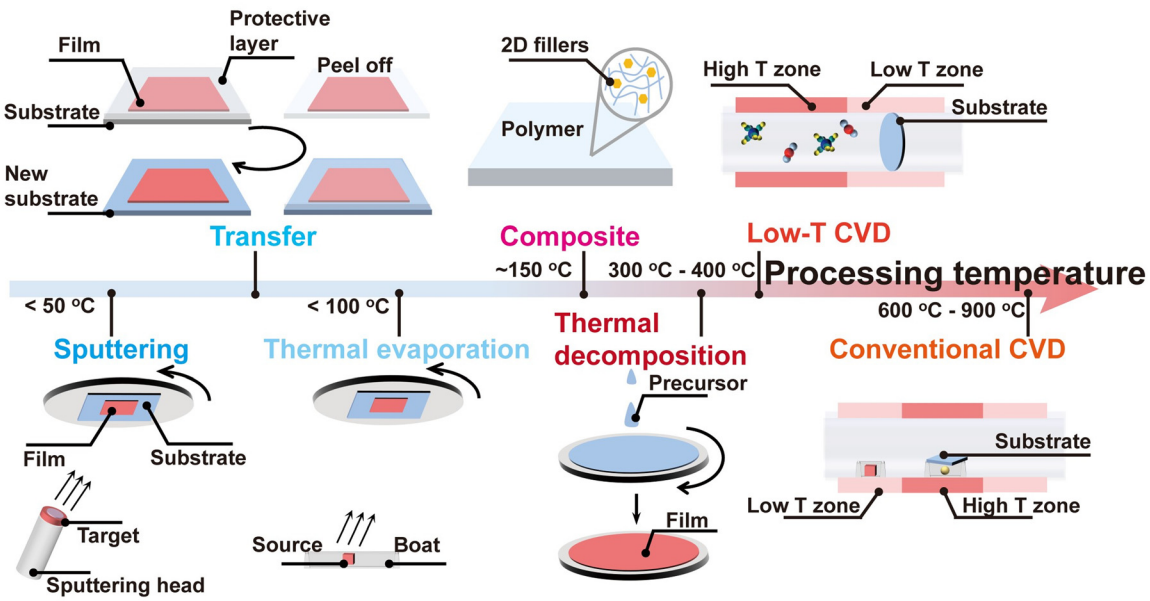

Fig. 3 Comparison of different preparation methods for 2D materials with a focus on the processing temperature.

deposition (ALD) are promising in directing 2D material's growth onto polymeric substrates, suppressing the contamination and unwanted defects/damages during the transfer process.[8,55] For example, MoS_2 can be deposited under 300 °C *via* low-T CVD and ALD, which is compatible with the back-end-of-line (BEOL) integration and soft robot integration.[14] Despite the successful attempts, the increased defect density (mainly grain boundaries) might be detrimental for some applications although the thickness and crystallinity of deposited films are still high. Overall, each fabrication technique has its unique advantages and disadvantages (Table 1), and the best process should be selected based on actual requirements.

Several factors still impede the further deployment of 2D materials in soft robotics. The primary issue is effectively scaling up the fabrication of 2D materials with acceptable defect density. The promising roadmap for fabrication is discussed in the perspective part. The second limitation is the durability of the integrated devices based on 2D materials. Key factors leading to the poor durability of devices primarily include the limited stability of 2D materials in a harsh environment with high temperature and/or high humidity, in which the mismatch of thermal expansion coefficients between 2D materials and the supportive substrates affects the film stability. Encapsulation is a simple but effective method to prevent potential oxidation and unwanted water absorption. Hence, a light-transparent, flexible encapsulation layer with high dielectric coefficient is preferred to endure the responsiveness of 2D materials. Among the encapsulation materials, PDMS, styrene–ethylene–butylene–styrene (SEBS) and parylene are promising for protecting 2D materials.[61–63]

For the energy transducers in soft robots (mainly actuators), the failure in devices based on 2D materials can be primarily attributed to their structural defects and the interaction with polymer substrates. Their structural defects such as vacancies, dislocations, and grain boundaries act as stress concentrators, in turn, leading to mechanical failures.[64] The mismatch in elastic moduli can induce mechanical failures in those applications where 2D materials are integrated with polymer substrates. As the polymer substrate deforms, it can impose strains on the 2D material, leading to crack initiation and propagation.[65] Self-healing materials and fatigue-resistant polymer supportive networks are promising to address these challenges.[66]

3. Two-dimensional materials for actuators in soft robots

Soft actuators leveraging flexibility and conformability exhibit the ability to manipulate fragile objects and operate in complex environments. The key factors influencing the performance of soft actuators include actuation force, actuation power, and actuation speed. These factors are determined by the material selection, actuation mechanism, and device structure of the actuator. In general, the untethered soft actuators include pneumatically/hydraulically driven soft actuators, magnetic-driven soft actuators, electrically driven soft actuators, and heat-driven soft actuators.[5] The research in this field has shifted from improving its simple motion performance to the direction of miniaturization, dexterity and intelligence. Herein, we review the role of 2D materials in the soft actuator field with a focus on their actuation mechanisms and functional applications. At the conventional soft actuator frontier, Li *et al.* highlighted soft actuator performance metrics, and Jung *et al.* reviewed the untethered soft actuators for soft standalone robotics by introducing the state-of-the-art soft actuators under different stimulation modes.[5,67]

3.1 Actuation mechanisms for 2D materials

The unique properties of 2D materials such as high surface-to-volume ratios, mechanical flexibility, and tuneable electronic/thermal conductivities have revolutionized actuation mechanisms in soft robotics. These materials enable energy-to-motion conversion across diverse stimuli including electrical, thermal, chemical, humidity and optical inputs. These actuation processes can be categorized to microscale actuation and macroscale actuation in terms of their actuating force.

Atomically thin 2D flakes with microscale area can be actuated by optical or electrostatic stimuli to move on the horizontal surfaces. Optical actuation refers to a mechanism in soft robotics where light energy (*e.g.*, visible, infrared, or ultraviolet radiation) is converted into mechanical motion or deformation in an actuator. For example, 2D VSe_2 and $TiSe_2$ nanoflakes were actuated by femtosecond pulsed laser to achieve movement on sapphire and quartz substrates with large vdW interactions in between (Fig. 4a).[68] The actuation is attributed to the surface acoustic effect and thermal stress, which unfortunately has been proved unworkable in other 2D TMD materials. This actuation mechanism with non-touch and non-invasive properties offers potential in drug delivery and biology applications. Ultrathin 2D flakes are used in electrostatic actuators leveraging their exceptional electrical conductivity, enabling micro actuator applications in micro-electromechanical systems (MEMS). Electrostatic actuation is a mechanism to attract or repel actuating component by electrostatic forces. For example, a micro-scale graphite flake (15×15 μm^2) was actuated by an applied DC voltage and the moving direction could be adjusted by changing the form of applied voltage, showing a robust reliability over 10 000 reciprocating actuation cycles (Fig. 4b).[69]

Generally, microscale actuators are suited for various applications such as microsurgery,[70] imaging, sensing,[71] drug delivery[72] and lab-on-chip devices.[73] Their small size, non-touch actuation, and compliance allow for gentle interaction with fragile biological materials without causing damage. The development of lithographic techniques and novel material platforms enables microrobots, artificial cilia, and cell-scale manipulation.[74] Drug delivery is one of the promising applications in this field due to the increasing demand for efficient therapy. Microscale actuators can serve as active platforms to deliver and release drug, thereby significantly accelerating the process in comparison with traditional targeted drug delivery

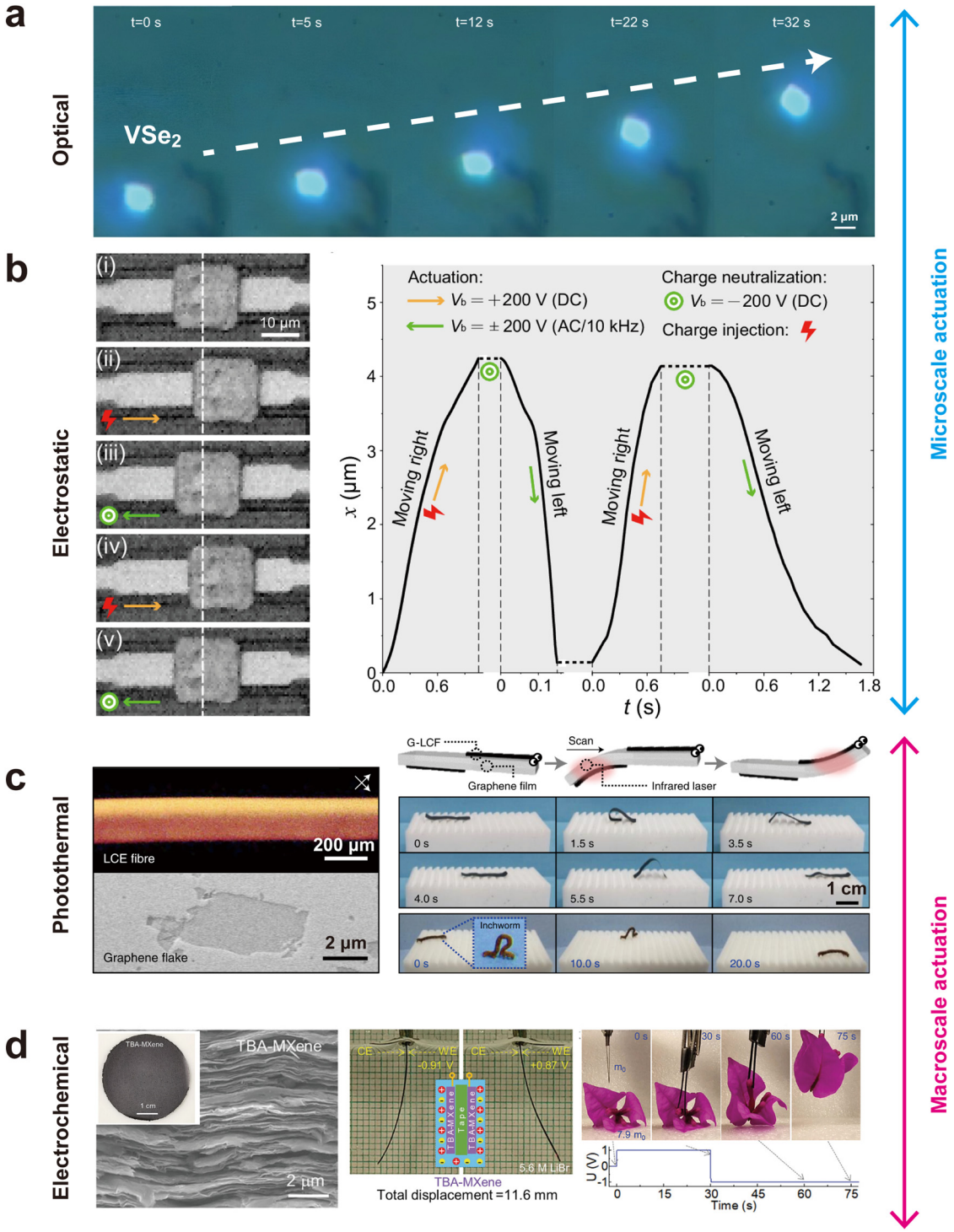

Fig. 4 Various actuation mechanisms for 2D materials. (a) Optical actuation. Reproduced with permission.[68] Copyright 2023, Springer Nature. (b) Electrostatic actuation. Reproduced with permission.[69] Copyright 2025, Springer Nature. (c) Photothermal actuation. Reproduced with permission.[11] Copyright 2025, Springer Nature. (d) Electrochemical actuation. Reproduced with permission.[77] Copyright 2024, John Wiley and Sons.

systems, which relies on the fluxes of blood and diffusion. For example, a reduced nanographene oxide (n-rGO)-based electrochemical actuator was reported to achieve ultrafast release of doxorubicin (DOX) at the tumor site within a few seconds.[72] In addition, microscale actuators can be used as pumps and valves in microfluidic systems for lab-on-chip (LoC) systems. LoC platforms with small size and reduced costs enable the fast analysis in medical applications.[75] Microscale actuators are required to control the flow of various liquids (buffer, drug, *etc.*) at microscale by performing as microvalves. For example, an actuator based on GO–hydrogel composites was developed to block the channels in LoC systems. Upon optothermal

Table 2 Comparison between different actuation mechanisms for 2D materials and pneumatic actuation (which is typically based on polymeric materials)

Actuation mechanism	Scale	Deformation (strain)	Blocking force	Speed	Materials	Ref.
Optical actuation	Micro/nanoscale	Low to moderate	<5 mN	Very fast ($<$ ms)	Graphene, TMDs	68
Electrostatic actuation	Micro/nanoscale	Low	$\sim$50 nN	Very fast (μs–ms)	Graphene, h-BN, TMDs	69
Photothermal actuation	Micro- to macroscale	Moderate	4.1 N with 100 strand bundling	Fast (ms to s)	Graphene, MoS_2, WS_2, black phosphorus	11
Joule thermal actuation (electrothermal actuation)	Micro/nanoscale	Moderate	5 mN	Moderate (s)	Graphene, MXenes	77 and 82
Electrochemical actuation	Micro- to macroscale	High	0.5–10.0 mN	Slow (s to min)	Graphene oxide, MXenes	77 and 83
Pneumatic actuation	Macroscale	High	1–100 N (depending on the pressure and the contact area)	Moderate (s)	N/A	84 and 85

heating with a laser, the actuator reduces its volume to open a flow of solutions at microscale. Moreover, the flow rate can be adjusted between 10 and 20 μL min^{-1} by adjusting the power supply of the light source.[73]

Unlike microscale actuators, macroscale actuators provide programmable bending, folding and grasping with substantial deformation and blocking force in soft robots. The high deformation at the macroscale requires the preparation of large-scale 2D materials and their integration into devices. Photothermal actuation and Joule thermal actuation are widely applied to fabricate artificial muscles. Light-responsive graphene and MXenes are used in photothermal actuators due to their broad light absorption spectra.[18,76] A single-fibre actuator with graphene fillers was demonstrated as an artificial worm to self-crawl by photothermal actuation (Fig. 4c).[11] Moreover, a 1000-strand bundle of fabricated fibres was able to lift a 1 kg dumbbell, showing supreme high actuation power. Electrochemical actuation, based on the movement of ions (*e.g.*, Li^+, H^+, or OH^-) into or out of a material, causes volume changes and also offers macroscale actuation with a relatively low voltage applied. Chen *et al.* developed a large-scale TBA-functionalized MXene-based film with a peak-to-peak strain difference of 0.771% under a voltage of $\pm$1 V, demonstrating a macroscale actuation by lifting objects effectively (Fig. 4d).[77]

Table 2 summarizes the key parameters of various actuation mechanisms for 2D materials. Each actuation mechanism exhibits unique advantages that can be tailored to specific applications. Optical and electrostatic actuation are ideal for high-speed and precision tasks at microscale, while photothermal and Joule thermal approaches offer balanced performance for flexible electronics and wearable devices at macroscale. Electrochemical actuation, though slower, delivers high deformation, making it highly suitable for artificial muscles.

3.2 Functional applications enabled by 2D material-based actuators

The development of soft actuators is to design moving parts similar to biological limbs to achieve various movement modes with flexibility and conformability. Inspired by terrestrial organisms, crawling and jumping soft robotics are integrated by 2D materials.[78,79] Fig. 5a shows the NIR light–driven worm-like MXene-based robot through an asymmetric structure design, leveraging the decent photothermal actuation performance of MXenes. Stimulated by the alternative on/off process of the NIR light, the two ends of the worm robot unidirectionally walk with a step of 5 mm. Given a more complex device design, multidirectional movement can be achieved for the crawling robots.[80] Inspired by larva, a robot can jump as high as 41 mm, which is 10.3 times its own height. The jumping mode is achieved by the storage and instantaneous release of elastic deformation energy under light irradiation of a MXene composite film. This bio-mimic design also enables an adjustable jumping direction by simply tuning the light irradiation angle (Fig. 5b).[81]

Leveraging the outstanding electrochemical and photothermal actuation performance of 2D materials, such as graphene and MXenes, swinging and flying robots are integrated. Umrao *et al.* reported an ionically cross-linked $Ti_3C_2T_x$ electrode for artificial muscle with an ultrafast response time within 1 s and decent durability of 97% up to 18 000 cycles. Based on the robust performance of the artificial muscle, ''dancing'' butterflies with moving wings can be fabricated (Fig. 5c).[86] Inspired by the vine maple seed, Wang *et al.* reported a rotary flying photoactuator (actuated under near-NIR light) with a rapid response of around 650 ms and an ultrafast rotation speed of $\sim$7200 rpm, enabling controlled flight and steering behaviors (Fig. 5d).[87] This can be attributed to the synergistic interactions between the photothermal graphene and the hygroscopic agar/silk fibroin components. The key parameters for the flying motion, such as rotation speed, flight height and flight direction, can be controlled by varying the irradiation intensity and position. This flying robot is expected to be deployed in unstructured environments for high-resolution aerial digital imaging.

Soft grippers attract intensive attention due to their light weight, high weight-to-gripper ratio and flexibility, enabling grasping, fragile objects in particular, for intelligent sorting and adaptive gripping. Although most studies focus on pneumatic grippers, the cumbersome pump and complicate gas tubes might not be suitable for a complex environment, especially small space. Therefore, 2D materials show potential in soft grippers due to their non-contact actuation mechanisms,

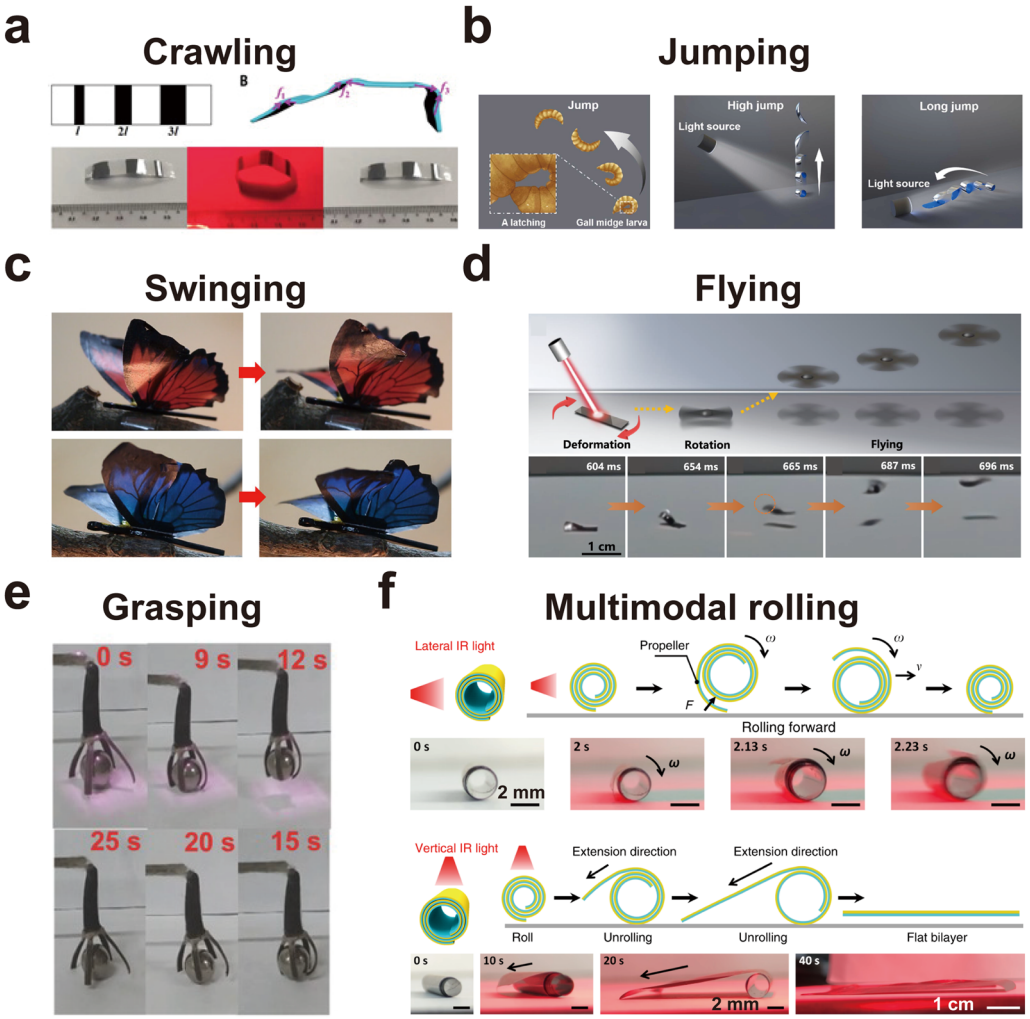

Fig. 5 Various functional applications enabled by 2D material-based actuators. (a) Crawling. Reproduced with permission.[80] Copyright 2019, AAAS. (b) Jumping. Reproduced with permission.[81] Copyright 2022, Elsevier. (c) Swinging. Reproduced with permission.[86] Copyright 2019, AAAS. (d) Flying. Reproduced with permission.[87] Copyright 2023, Springer Nature. (e) Grasping. Reproduced with permission.[88] Copyright 2017, John Wiley and Sons. (f) Multimodal rolling. Reproduced with permission.[89] Copyright 2020, Springer Nature.

such as photothermal conversion. For example, a WS_2-based gripper can lift a steel ball with a weight 500 times heavier than the gripper itself (Fig. 5e).[88] This high griping force can be attributed to the effective exfoliation of WS_2 in sodium alginate, which, in turn, ensures tunable filler-loading levels in their composites without aggregation.

Unlike the bio-inspired motions, rolling robot, usually in cylindrical geometry, refers to roll autonomously under a stimulus, offering significant potential in conveyors and motors. This motion is driven by an unstable center of gravity under an external stimulus. Fig. 5f shows the rolling robot with a double layer of stacked graphene assembly and polyethylene film. Under lateral IR irradiation, the robot can roll with an increasing rolling speed due to the localized photothermal effect of the propeller. Under vertical IR irradiation, the robot will uncoil instead of roll due to the design of the structure. The rolling robot triggered by non-contact irradiation is expected to work on a wavy sandy ground.[89]

4. Two-dimensional materials for human–mimic perceptions

The rapid advancement of flexible electronics has opened new frontiers in the development of sensors that can mimic the human–mimic perceptions, enabling applications such as soft robots, virtual reality (VR) and health monitoring wearable devices to interact with their environment in ways that have been previously unimaginable.[90–92] Among the promising materials for these applications are 2D materials, which offer exceptional mechanical flexibility, tuneable electronic properties, and high sensitivity to external stimuli.[93–95] These unique characteristics make 2D materials ideal for creating sensors that replicate the five senses—sight, hearing, touch, taste, and smell.

The fundamental approaches for sensors to mimic the five senses mainly revolve around piezoelectricity, piezoresistivity, capacitivity, triboelectricity, chemosensitivity, ion sensing,

photoconductor, phototransistor and photodiode (Fig. 6). In the following section, detailed working principles of each mechanism will be discussed. Additionally, Table 3 lists the overall comparison of each mechanism behind the perception sensors, highlighting the advantages and limitations of each approach.

Piezoelectric sensors work based on the piezoelectric effect, where it converts applied mechanical force into electrical voltage output. Piezoelectric effect was first discovered in 1880 by the Curie brothers in quartz.[96] It can exist as either a pressure or strain sensor, depending on the sensing material, as well as the device structure. Hence, piezoelectric sensors are highly responsive to dynamic mechanical changes, making them ideal for applications such as tactile and acoustic sensors.[97,98] Furthermore, due to their energy harvesting nature, piezoelectric sensors can

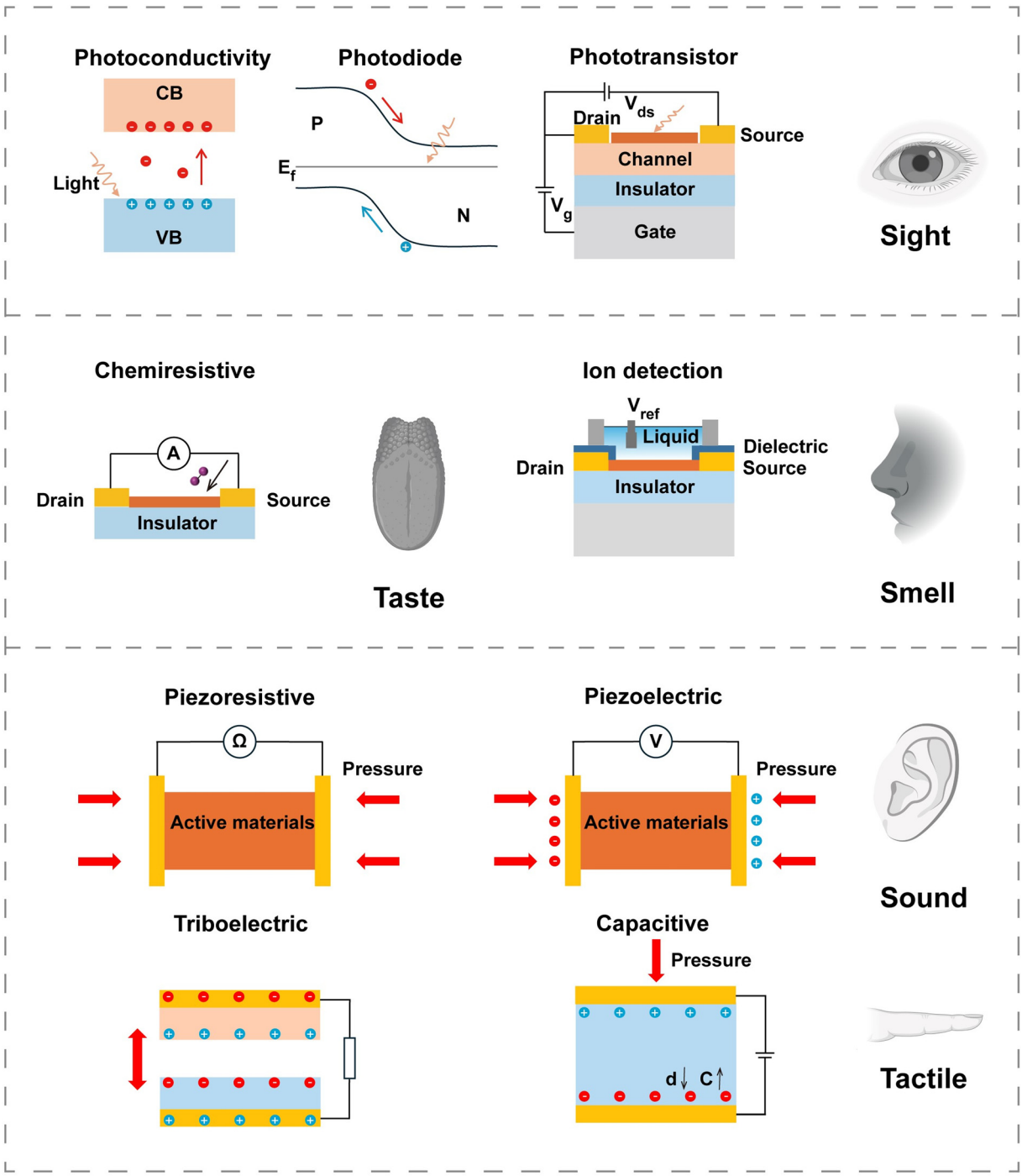

Fig. 6 Schematic of the different approaches to mimic human perceptions. Illustrations of human–mimic perceptions were created using BioRender: https://BioRender.com.

Table 3 Overall comparison of the sensing approaches for human–mimic perceptions

Perception	Approach	Advantages	Limitations
Vision	Photoconductor	Low power consumption	Possibility of suffering from high dark current when not properly shielded Limited response to certain wavelengths
	Phototransistor	High gain and sensitivity to light Improved signal-to-noise ratio due to amplified signals	Requires complex circuit Slow response time
	Photodiode	Fast response time High sensitivity to light Low power consumption	High cost to assemble device Limited dynamic range
Tactile	Piezoresistive	Easy fabrication High sensitivity to stress/strain Fast response time	Requires power to operate Signal output affected by external factors such as temperature Static sensing Low sensing frequency (0–10 kHz) Signal drift Lag effect
	Piezoelectric	Self-powered sensor High sensitivity to mechanical stress/strain High sensing frequency (10 Hz to MHz) High signal to noise ratio	Can only be used for dynamic sensing
	Capacitive	Easy fabrication Low power consumption Response to both dynamic and static stimuli Fast response time	Nonlinearity Susceptible to parasitic effects and electromagnetic interference Require careful electrode design Low sensing frequency (0–100 Hz)
	Triboelectric	Easy fabrication Self-powered sensor Wide selection of material Fast response time	Wear and tear of material can reduce performance High output impedance Low sensing frequency (3 Hz–10 kHz)
Sound	Piezoresistive	Easy fabrication High sensitivity to stress/strain Fast response time Low sensing frequency (0–10 kHz)	Requires power to operate Signal output affected by external factors such as temperature Static sensing Signal drift Lag effect
	Piezoelectric	Self-powered sensor High sensitivity to strain	High noise level
Olfactory	Chemiresistive	High selectivity to target chemical species Able to detect low gas concentration	Limited device lifespan Potential interference from other chemicals
Gustatory	Ion sensing	Detect ions in very low concentration High selectivity to ionic species	Drift over time and loss of selectivity

exist as self-powered sensors with no power consumption required.

Piezoresistive sensors work based on the principle of converting applied pressure into electrical resistance variation.[99] This effect is particularly pronounced in semiconductors such as silicon, where strain alters the mobility of charge carriers, thereby modulating resistivity. Different from piezoelectric sensors, piezoresistive sensors are static sensors. More than often, piezoresistive sensors are found in both tactile and acoustic sensor applications due to their fast response time. The resistance of the sensor can be calculated as follows:

$$R = \frac{\rho L}{A}$$

where R, ρ, L and A represents the resistance of sensor, resistivity of material, length and cross-sectional area, respectively.

The structures of capacitive sensors are usually composed of top and bottom electrodes sandwiched between a substrate and an insulator. When pressure is applied perpendicularly to the device, it resulted in a deformation of the active area, thus changing the distance between the two electrodes, hence capacitance change. Capacitive sensors have garnered extensive attention for flexible electronics, especially as a tactile sensor, due to their large detection range, high sensitivity, and minimal response to temperature drift. They are also suitable for a wide range of applications since they possess good sensitivity to both static and dynamic pressures, fast response time, and low power consumption. The capacitance of the sensor can be calculated as follows:

$$C = \frac{\varepsilon_0 \varepsilon_r A}{d}$$

where C, ε_0, ε_r, A and d represents the capacitance of sensors, vacuum permittivity, relative permittivity contact area of the electrodes, and distance between the electrodes.

Triboelectric sensors have been gaining research interest due to their wide material selection, simple configurations, and high output voltage. First proposed by Fan *et al.*, based on the mechanism of transducing mechanical energy into electrical signals through the coupling of the triboelectric effect, also known as contact electrification, and electrostatic induction.[100] Upon applying a mechanical compression, an electric potential difference between the top and bottom electrodes is produced, which results in a charge transfer between the two triboelectric material surfaces. Similarly, triboelectric sensors are mostly

presented as tactile sensors due to their high sensitivity and fast response time.[101–103] Furthermore, similar to piezoelectric sensors, triboelectric sensors can exist as self-powered sensors.

Chemiresistive sensors are based on the change in electrical resistivity caused by the adsorption of molecules on the surface of the sensing layer or metal electrodes.[104] These interactions, influenced by material type, properties of gas, temperature, pressure, and humidity, alter the electron density in the semiconductor. When a metal electrode contacts the semiconductor, their Fermi levels align, creating a Schottky barrier if their work functions differ. For n-type semiconductors, electron-donating gases such as NH_3 increase the electron density, thus reducing the resistance, whereas electron-withdrawing gases such as NO_2 decrease the electron density, thereby increasing the resistance. Conversely, p-type semiconductors exhibit the opposite behaviour. The Schottky barrier's height and depletion layer thickness depend on the work function difference and doping effects. Adsorbed gases also modify the semiconductor's Fermi level, shifting it toward the conduction or the valence band, thereby altering the built-in potential and resistance at the electrode-semiconductor junction. Generally, n-doping by reducing gases decreases the resistance in n-type materials but increases it in p-type materials, while p-doping by oxidizing gases has the reverse effect. This mechanism enables the detection of specific gases based on resistance changes. For example, the p–n heterojunction, *via* the incorporation of n-type 2D SnO_2 sheet and p-type black phosphorus, introduced oxygen vacancies, thereby amplifying the carrier concentration after the adsorption of H_2S. The BP–SnO_2 sensor exhibited a larger sensitivity than that of a pure SnO_2 sensor (1.3/ppm *vs.* 0.342/ppm), alongside faster response/recovery speeds.[105] Similarly, an rGO–MoS_2 composite formed a p–p heterojunction. The synergistic effect of MoS_2 and rGO significantly enhances the selectivity toward NH_3 compared to other gases by promoting the charge transfer and surface interaction.[106]

Ion sensing is a type of chemical sensor, which detects small organic or inorganic molecules or ions in the aqueous phase. The main mechanism is driven by the protonation and deprotonation of the functional group that is present on the surface of the 2D materials. It has a similar working mechanism as chemiresistive; however, instead of change in resistance, it is usually reflected by change in current or voltage output. For example, an MXene-based electronic tongue can detect the sourness by generating varying current signals when it is subjected to pH variation. The good performance of this MXene sensor is attributed to the abundant functional groups, mainly –OH, –F, and –O, on MXene surface, allowing effective ion sensing.[107] In addition to mimic gustatory and olfactory perceptions, this technique is applied to detect minute concentrations of chemicals in food. Glyphosate, a widely used herbicide, can be selectively detected by a CeO_2–graphene oxide chemical sensor with a detection limit of 30 nmol L^{-1}.[108]

Photoconductor is a device for which electrical conductivity increases upon exposure to light. It operates on the photoconductive effect, where absorbed photons generate electron–hole pairs, resulting in an increase in the number of charge carriers. This device has a lateral structure, which consists of an active layer and two electrodes, and is commonly used in optoelectronic devices, which can also be observed in several 2D material-based photodetectors such as 2D perovskites, TMDs, and graphene.[109–111] For example, the hybrid MoS_2–graphene photoconductor shows a ultrafast response of $\sim$17 ns and a high responsivity of $\sim 3 \times 10^4$ A W^{-1} at 635 nm illumination with 16.8 nW power across the broad spectral range. The excellent performance can be attributed to the addition of an MoS_2 layer with the abilities of tunnelling, as well as passivating surface states.[111] This improvement makes it promising for optoelectronic applications in soft robotics.

Phototransistor is a light-sensitive transistor that amplifies photogenerated current. It can be considered as an extension from photoconductor, whereby it combines the photoconductive effect with the gain mechanism of a transistor. With a similar working principle as the photoconductor, phototransistor can provide photogenerated carriers when exposed to light and form photocurrent *via* the conductive channel of the active layer, such as MoS_2 and 2D perovskites, driven by the source-drain voltage.[112,113] Akhil *et al.* reported a monolayer MoS_2 phototransistor array with a responsivity of $\sim 3.6 \times 10^7$ A W^{-1} and a high dynamic range of $\sim$80 dB. Interestingly, the MoS_2 phototransistor exhibited programmable phototransistor in each pixel, offering a substantial reduction in footprint and energy consumption. This reduction is attributed to the atomic thickness and multifunction nature of MoS_2.[112] Additionally, due to the gate voltage, the active layer can generate more photogenerated carriers, allowing the electrical signal to be further amplified. Therefore, upon comparison with photoconductors, phototransistors with a gate voltage display a higher external quantum efficiency and an on/off ratio. At the same time, the phototransistors have a slower response speed. For example, the response speed for graphene-based phototransistors was $\sim$400 ns, whereas its photoconductor counterpart ranged from 10 ns to 3 μs.[111,114,115]

Lastly, photodiode is a semiconductor device that converts light into an electrical current through the photovoltaic effect. Photodiodes typically exist as vertical devices, which are made up of functional layers sandwiched between the top and bottom electrodes. The photodiode uses the photovoltaic effect of semiconductors that usually work under a reverse bias voltage that promotes the electron–hole pairs to separate, therefore achieving a higher on/off ratio and a faster response speed. Despite the lower external quantum efficiency and responsivity as compared to phototransistors and photoconductors, photodiodes usually exhibit a large linear dynamic range and high detectivity due to the low dark current. Some 2D materials are commonly used as photodiodes including TMDs, black phosphorus (BP) and 2D perovskites.[116–120] Photodiodes can be self-powered due to their vertical structure, which reduces the carrier transport distance, thus facilitating a faster response speed and a lower working voltage.

By leveraging the extraordinary properties of 2D materials, researchers are paving the way for a new generation of soft robots that can perceive the world with human–mimic perceptions. Table 4 summarizes the 2D materials used for each

Table 4 Comparison of the 2D materials used for each perception sensor and their respective challenges

Perception	Materials	Challenges
Vision	Graphene TMDs 2D perovskites Black phosphorus	Stability under different wavelengths Long-term performance degradation
Tactile	Graphene TMDs MXenes Black phosphorous 2D perovskites	Long-term stability Sensor linearity output
Sound	Graphene TMDs MXenes 2D perovskites	Limited detection frequency range
Olfactory	Graphene TMD MXenes 2D MOFs	Selectivity of the gas ions/molecules Detection of unwanted gas ions with similar functional group
Gustatory	Graphene TMDs MXenes 2D MOFs	Sensitivity of the ions Long-term performance degradation of the sensor

perception sensor, at the same time highlighting the challenges they faced, respectively. These advancements not only enhance the functionality of soft robotic systems, allowing them to sense their surroundings with remarkable sensitivity.

Among the five perceptions, vision and tactile are most attractive for soft robots to depict their working environment in real time by capturing and monitoring signals continuously. Further, robots can react and respond to any changes in environments by actuating the motion components, such as circumvent obstacles and grasping objects, if a closed-loop system is equipped. Sensitivity, detection limit and wavelength/frequency range of vision and tactile sensors are primary parameters determining the use case in a soft robot. For example, tactile sensors with a low detection limit are required for monitoring minute strain/deformation (*e.g.*, slippage detection), while tactile sensors with high sensitivity are suitable for circumstances with indistinguishable stimuli (material/texture recognition).

Unlike vision and tactile sensors, which are often needed in soft robots, the other three perceptions are only deployed in certain situations (*e.g.*, gather information about sounds and molecules). Although the mechanisms for tactile and sound perceptions are almost same, the performance stability varies. The primary difficulty lies on sound perception is the signal-to-noise ratio due to the non-contact sensing, which is susceptible to external noise. However, noise is commonly derived from soft robots (*e.g.*, pump and motor) and their working environments. The capability to differentiate signal with a wide detection frequency range is indispensable to solve this issue. Similarly, supreme selectivity of molecules is important for olfactory and gustatory sensing in soft robots.

4.1 Vision

Optical sensors are often employed to recognize and distinguish an object using light. Therefore, optoelectronic devices are often integrated to mimic the function of the eye. An optical sensor uses vision to detect changes in the amount of light incident, intensity and wavelength. The main device structures are based on intrinsic semiconductor properties, which are generically termed photoconductors, phototransistors, and photodiodes. In the case of 2D-based artificial vision, phototransistors and photodiodes are more common. Table 5 summarizes the list of 2D materials used in optical sensors, comparing the key parameters against the commercial sensor.

Two-dimensional materials such as graphene, MXenes, TMDs, and 2D perovskites are widely used as optoelectronic materials owing to their semiconductor properties.[121–124] Currently, there are a wide variety of 2D-based photodetectors fabricated with a detection range from ultraviolet to the near-infrared reported.[125–128] Graphene is the first and highly researched 2D material that exhibited extremely high carrier mobility, high electrical conductivity, wide absorption from ultraviolet to terahertz, and a bandwidth of 40 GHz.[129–131] For example, Xu *et al.* reported a graphene derivative, GO-based for flexible artificial system with 81% accuracy in image recognition *via* the photoconductive effect.[132] Liang *et al.* also reported that the use of graphene helped to reduce the relaxation time as the conductivity of the artificial vision system increased.[133] This reduction of relaxation time is significant as it allows the artificial synapses to achieve short-term plasticity.

The zero bandgap and ultrahigh carrier mobilities at low temperatures of graphene enable its detection from the visible to terahertz range. However, single-layer ''zero bandgap'' graphene exhibits large dark current and poor absorption of light, thus limiting its practical applications. This results in a shift of research interest towards other 2D materials such as TMDs of decent mobility and strong light coupling from vis to mid-IR.[122]

As an emerging group of 2D materials, 2D perovskites possess excellent optoelectronic properties, which are especially observed in the field of photovoltaics.[134]

Table 5 Comparison of commercial sensors and reported 2D materials used in optical sensing

Materials	Response time	Photoresponsivity	Stability	Ref.
Commercial sensor	0.0125–33 μs	0.006–0.72 A W^{-1}	—	https://www.hamamatsu.com/
2D perovskite	5–50 s	—	—	140
2D perovskite	—	10^4 A W^{-1}, visible light 200 A W^{-1}, NIR	—	141
2D perovskite/graphene	0.08 s	730 A W^{-1}	74 days	142
h-BN encapsulated graphite/WSe_2	—	Up to 2.2 × 10^6 A W^{-1}	—	143
Ta_2PdS_6/MoS_2	470 ms	590.36 A W^{-1}, 633 nm	—	144
MoS_2	—	∼3.6 × 10^7 A W^{-1}	—	112
MoS_2/graphene	2.7–6.1 s	23.95 A W^{-1}, 532 nm, strained condition	10 days	145
MoS_2/black phosphorus	4.8 μs	Up to 110.68 A W^{-1}	—	146
MoS_2	0.044–0.119 s	Up to 119.16 A W^{-1}	—	147
MXene	—	0.07 A W^{-1}	—	148
PbS QD/MXene	30 ms	1000 mA W^{-1}	Bending: 500 cycles	149
Quasi-2D perovskite-MXene	—	∼151 A W^{-1}	>50 cycles	150
Black phosphorus	—	—	Bending: 100 cycles	151
Black phosphorus/graphene/InSe	24.6 ms	Up to 3.02 × 10^4 A W^{-1}	—	152

Two-dimensional perovskites exhibit low defect density, high carrier mobility, strong light absorption, and ease of fabrication, making them promising candidates for flexible and highly performing photodetectors.[127,135–137] Wang *et al.* reported on the use of quasi-2D halide perovskite photodetectors for optical imaging.[138] Its performance was comparable to its 3D derivative, $MAPbI_3$ photodiode. Furthermore, the performance of the photodetector was stable even after 100 days of storage under ambient conditions, in the presence of both air and humidity, which was something 3D perovskites cannot achieve thus far. Generally, large organic cation spacers are added to separate octahedral layers to form 2D perovskites.[139] The improved stability in air and humidity is attributed to the hydrophobic groups of aromatic or alkyl amines in large organic cation spacers such as butylammonium. This shows the potential of 2D perovskites in optical sensing applications. Wang *et al.* also demonstrated artificial retina using 2D perovskites for facial recognition purposes with high accuracy (Fig. 7a).[140]

To enhance the performances of the optoelectronic devices, heterostructures of the 2D materials are fabricated to tune the material's property. Seo *et al.* reported an optic-neural synaptic device based on h-BN and WSe_2 heterostructures developed by integrating synaptic and optical-sensing functions in a single device (Fig. 7b).[153] Polat *et al.* also reported a flexible graphene-based photodetector as a wearable fitness monitor and a UV sensor, where PbS quantum dots were applied as sensitizers to improve the UV-IR responses.[154] Zhang *et al.* demonstrated the growth of heterostructures perovskite/graphene, which achieved a high responsivity of ∼10^7 A W^{-1}. With the exceptional high-responsivity photodetector, it can be incorporated into flexible substrates as image sensors.[155]

However, the key issue with optical sensors is the time-lag response. This time-lag response occurs due to the limited response speed of light absorption and emission in certain 2D materials such as MoS_2 or 2D perovskites, which exhibit a lower carrier mobility than that of the other semiconductors. The lower carrier mobility can be attributed to enhanced quantum confinement and reduced dielectric screening, which lead to stronger Coulomb interactions and the formation of tightly bound excitons.[156–158] In 2D materials such as MoS_2, the energy level separation increases with the reduction in thickness due to quantum confinement, where the motion of charge carriers is restricted in one or more dimensions, leading to discrete energy levels. This results in inefficient phonon emission by hot carriers, thus causing a phonon bottleneck effect. The carriers can relax *via* emitting optical phonons only with the energy or sum of them equal to that of the energy gap, leading to slower carrier recombination.[159,160] For MoS_2, it possesses low carrier mobility (1 cm^2 V^{-1} s^{-1}) and indirect bandgap for multilayers, while the carrier mobility can increase to 122.6 cm^2 V^{-1} s^{-1} for single crystal monolayers after optimizing the preparation recipe.[52] Despite the significant improvement, its carrier mobility is still lower than that of traditional semiconductors such as silicon (1350 cm^2 V^{-1} s^{-1}).[161,162] Similarly, 2D perovskites exhibit a similar trend. Upon the addition of large organic cations butylammonium and phenethylammonium, there is a mismatch in dielectric constant between the bulky organic cations (ε = ∼4) and the inorganic octahedral layers (ε = ∼7.3), resulting in the formation of quantum wells.[163] Furthermore, the large organic cations hinder the carrier mobility between the octahedral layers due to their insulating nature.[164,165] Milot *et al.* reported a reduction in carrier mobility upon the addition of phenethylammonium cations (PEA^+) to $MAPbI_3$, where the carrier mobilities for $MAPbI_3$ and $(PEA)_2PbI_4$ were 25 cm^2 V^{-1} s^{-1} and 1 cm^2 V^{-1} s^{-1}, respectively.[166] This low carrier mobility hinders the sensor to rapidly detect changes in light intensity, particularly in high-speed or dynamic environments.

4.2 Tactile

Sense of touch, often referred to as a tactile system, perceives pressure and modes. It is critical for dexterity and interaction, which can be emulated using flexible pressures and strain sensors. The tactile sensors are transducers that obtain tactile information and convert them into electrical output signals, thus facilitating the recognition of texture, weight, and shape.

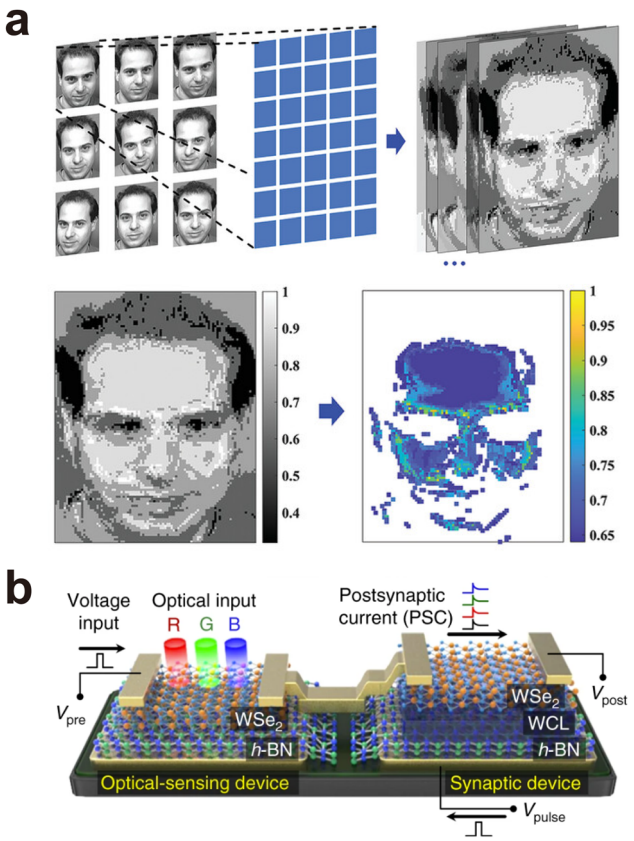

Fig. 7 2D materials for vision perception. (a) Artificial retina based on 2D perovskites with high recognition accuracy. Reproduced with permission.[140] Copyright 2024, John Wiley and Sons. (b) Representative illustration of the h-BN/WSe_2 synaptic device. Reproduced with permission.[153] Copyright 2018, Springer Nature.

As mentioned earlier, the primary working mechanisms for pressure sensors consist of piezoelectricity, piezoresistivity, triboelectricity and capacitivity. Table 6 summarizes the list of 2D materials used in tactile sensors, comparing the key parameters against the commercial sensor.

There is a wide material selection to assemble a piezoresistive device, with semiconductors exhibiting higher piezoresistive effects, thus making the 2D material a potential candidate for piezoresistive sensing applications.[167] Among the 2D materials, graphene is an ideal material for piezoresistive sensors due to its high conductivity, superior flexibility, large surface area, and robust mechanical strength.[168] Niu *et al.* reported the use of graphene as a flexible piezoresistive tactile sensor for both pressure and strain detection.[169] Similarly, Luo *et al.* demonstrated a 3D hollow structured graphene-based strain sensor with a good sensitivity of 15.9 kPa^{-1} and a faster response time.[170] Other 2D materials used as piezoresistive sensors include TMDs, where Ji *et al.* demonstrated MoS_2-based piezoresistive sensors.[171] Tannarana *et al.* also reported the assembly of a highly stable and high responsivity-functionalized $SnSe_2$ as a piezoresistive sensor (Fig. 8a).[172]

Piezoelectric materials are required to have a non-centrosymmetric crystal structure. Among the 2D materials, TMDs are known to exhibit large in-plane piezoelectricity.[188,189] Kim *et al.* reported a flexible single-crystal monolayer MoS_2 flexible strain sensor with an in-plane piezoelectric coefficient as high as 3.78 pm V^{-1}.[190] However, graphene and h-BN possess a centrosymmetric crystal structure. To further attain piezoelectric performance, surface engineering of these materials is required. For example, in the case of the graphene-based sensor, Chen *et al.* reported the use of heterostructures on the graphene-based sensor.[192] This heterostructure led to the surface modification of graphene, resulting in the breaking of the centrosymmetric crystal structure, thus successfully bringing the response time of the piezoelectric sensor to as low as 5 ms. Similarly, Tan *et al.* demonstrated a large piezoelectric effect in MXene-based sensors by oxygen-functionalized MXenes.[193] Two-dimensional perovskites have been reported to be promising piezoelectric materials. Upon the addition of the large organic cation spacers, it breaks the centrosymmetric structure of the perovskite, which favors piezoelectricity. Furthermore, in quasi-2D perovskites, there is an enhancement in piezoelectricity as compared to its 3D counterpart due to the presence of defects.[194] Ji *et al.* demonstrated the use of 2D halide perovskite, $(CHA)_2PbBr_4$, as a piezoelectric sensor with good voltage output linearity ($\sim$2.5 V N^{-1}, estimated from data) at a low applied pressure (1–5 N with an active area of 1 cm by 1 cm).[178]

However, for triboelectric sensors, materials with high electronegativity and electrical conductivity are suitable, as the large potential differences and high currents result in better signal outputs. Furthermore, the surface roughness of the material also plays a critical role, since friction between the material surfaces causes electron transfer. Therefore, Zhang *et al.* assembled an MXene-based triboelectric tactile sensor with leather to increase the surface roughness.[195] Ghosh *et al.* also reported a stretchable MXene-based triboelectric nanogenerator.[196] Guo *et al.* even demonstrated a laser-induced graphene-based triboelectric tactile sensor array, that can achieve pattern recognition and tactile imaging with high device performance stability (Fig. 8b).[191] Other 2D materials reported in triboelectric devices are 2D conductive MOFs, as reported by Wu *et al.*[197] With high electrical conductivity, 2D Cu-MOFs exhibited potential candidates in triboelectric sensors.

Lastly, the material selection to assemble a capacitive sensing device is high electrical conductivity to increase the dielectric constant of the sensing material. Zhang *et al.* reported MXene-based tactile sensors with high permittivity and low dielectric loss.[198] Mukherjee *et al.* also reported the use of printed flexible graphene as a cognitive gripper integrated onto a soft gripper, which facilitated slippage-free and damage-resistant gripping without interference from users.[199]

The introduction of 2D materials as fillers into a polymer is a common technique to improve the tactile sensor performance. Umapathi *et al.* demonstrated the use of an h-BN composite film as a pressure sensor, which can effectively detect handwritings.[200] The addition of h-BN into PDMS enhanced the output voltage to $\sim$198.6 V and a maximum peak power density of 7.86 W m^{-2}. Yang *et al.* also introduced

Table 6 Comparison of the commercial sensor and reported 2D materials used in tactile sensing

Materials	Response time	Detection range	Sensitivity	Stability	Ref.
Commercial sensor	<5 ms	0–5 MPa	—	>1 million times	https://Flexniss.com
Commercial sensor	<5 μs	4.4 N 111 N 445 N	—	>3 million times	https://tekscan.com
PDMS/MXene	—	10–80 Pa 80–800 Pa	0.18 V Pa^{-1} 0.06 V Pa^{-1}	—	173
MXene	70 ms	Up to 117.5 kPa	3.94 kPa^{-1}	>7500 cycles	174
MXene nanocomposite	160 ms	Up to 500 kPa	Gauge factor (0–60% compression): 0.4 Gauge factor (60–80% compression): 2.61 Gauge factor (80–90% compression): 1.04	>6700 s	175
MXene/MOFs	15 ms	0.0035–100 kPa	110 kPa^{-1}	13 000 cycles	176
MXene/MoS_2	385 ms	1.477–3.185 kPa	14.7 kPa^{-1}	~2500 cycles	177
2D perovskite	—	1–5 N	—	4000 cycles	178
MoS_2/PDMS	30–50 ms	<1 kPa 1–23 kPa	150.27 kPa^{-1} 1036.04 kPa^{-1}	10 000 cycles	179
MoS_2–rGO based	—	0.5–5 N	7.5 V Pa^{-1}	100 cycles	180
MnO_x/MoS_2	<2 ms	0–45 kPa 45–150 kPa 150–1000 kPa	6601 kPa^{-1} 58 843 kPa^{-1} 22 812 kPa^{-1}	10 000 cycles	181
h-BN	15 ms	0.05–450 kPa	261.4 kPa^{-1}	>5000 cycles	182
Borophene	90 ms	0–1.2 kPa 1.2–25 kPa 25–120 kPa	2.16 kPa^{-1} 0.13 kPa^{-1} 0.07 kPa^{-1}	>1000 cycles	183
Black phosphorus	200 ms	<1 kPa 2–40 kPa 40–100 kPa	0.06 kPa^{-1} 0.02 kPa^{-1}	2800 cycles	184
Laser-induced graphene	12 ms	0–7 kPa 65 Pa–1000 kPa	52 260.2 kPa^{-1}	10 000 cycles	185
Vertical graphene	—	0–21.5 N	0.1–1.1 N	>25 200 cycles	186
Graphene	9 ms	0.2 Pa–425 kPa	2297.47 kPa^{-1}	>10 000 cycles	187

h-BN into an ionic ink, which enhanced the conductivity of the composite film, thus increasing the performance of the capacitive sensor (Fig. 8c).[182] Similarly, Rana *et al.* reported the enhancement of triboelectric sensor performance upon the addition of zirconium-MOFs and hybridized MXenes.[201] Kundu *et al.* also reported the addition of 2D TMOs into PVDF to enhance the piezoelectric properties of the sensor, thus enabling better identification of the shape and size of the object placed onto it.[202]

However, 2D material-based tactile sensors are also facing the issue of time-lag response. This issue surfaced due to the inherent mechanical properties of the materials and the signal processing mechanisms involved. For example, when 2D materials such as graphene or MoS_2 are subjected to compression or stretching deformation, there might be a delay in the real-time transfer of stress or strain information to the sensor's electrical output. Such phenomenon is mainly observed in a composite film, where 2D materials act as fillers. Nuthalapati *et al.* assembled a piezoresistive pressure sensor by embedding rGO in PDMS, where a delay in recovery time (58 ms) was observed.[203] The delay in recovery time was due to the viscoelastic property of the polymeric matrix.[204] Such observation is not unique to piezoresistive sensors, and other tactile sensors such as capacitive sensors also face the similar issue. A lag time (a response time of ~45 ms *versus* a recovery time of ~83 ms) has been observed due to the reconstruction of the percolation network in the polymer matrix after release of applied pressure or strain.[205,206]

The amount of applied pressure plays another key factor in influencing the response speed. In a high-pressure regime, larger deformation is generated, thus requiring a longer time to response and recover from original configuration, resulting in time-lag in tactile responses. For example, the response and recovery times under a pressure of 3 Pa were 37 ms and 14 ms for an rGO-based piezoresistive tactile sensor. However, the response and recovery times increased to 305 ms and 165 ms, respectively, when the applied pressure increased to 2634 Pa.[207]

4.3 Sound

Inspired by eardrum, acoustic sensors used to detect sound by receiving the vibration of air are called artificial eardrums. Other than artificial eardrums, acoustic sensors include voice recognition applications that are inspired from throat. Unlike artificial eardrum which recognizes sound from the vibration of air, artificial throat recognizes sound from the movement of the throat by either pressure or strain sensors. Similar to tactile sensors, piezoelectric and piezoresistive sensors are used in both artificial eardrums and artificial throat. Table 7 summarizes the list of 2D materials used in acoustic sensors, comparing the key parameters against the commercial sensor.

Gou *et al.* reported a piezoresistive MXene-based artificial eardrum that can detect human voice with high sensitivity and speech recognition accuracy.[208] In recent years, perovskites have been attracting attention for being promising piezoelectric

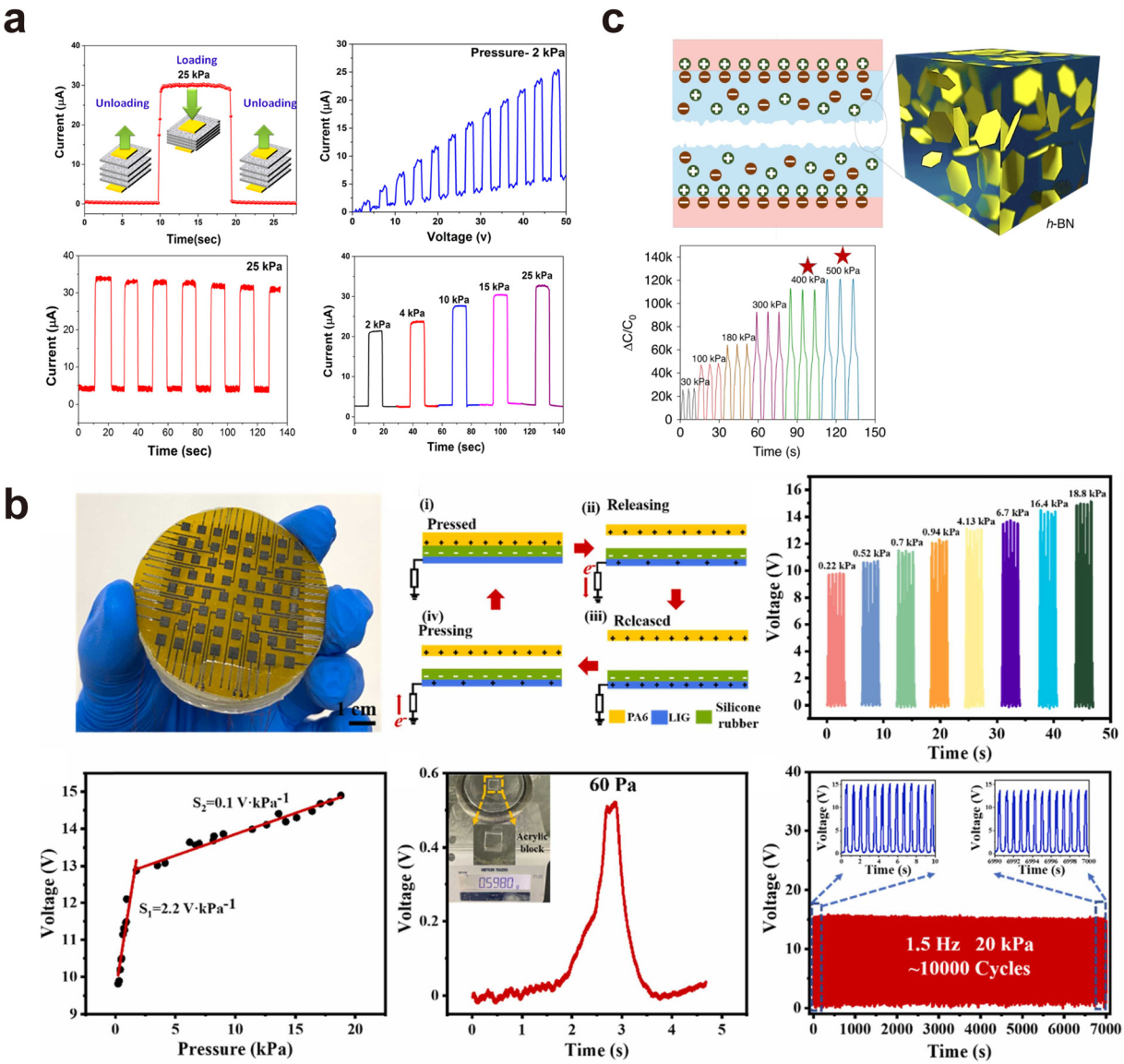

Fig. 8 2D materials for tactile perception. (a) Piezoresistive sensor based on 2D $SnSe_2$ with different pressures. Reproduced with permission.[172] Copyright 2023, Elsevier. (b) Image and working mechanism of the laser-induced graphene-based triboelectric tactile sensor, along with its sensing performance at different pressures. Reproduced with permission.[191] Copyright 2023, Elsevier. (c) Schematic of the h-BN-based capacitive tactile sensor, along with its device performance. Reproduced with permission.[182] Copyright 2023, Springer Nature.

Table 7 Comparison of the commercial sensor and reported 2D materials used in acoustic sensing

Materials	Response time	Detection range	Sensitivity	Stability	Ref.
Commercial sensor	—	50 Hz–20 kHz	52 dB	—	https://ca.robotshop.com/
MXene/MoS_2	~4 ms	40–3000 Hz	25.8 mV dB^{-1}	—	217
MXene/bacterial cellulose	90 ms	0–0.82 kPa 0.82–10.92 kPa	51.14 kPa^{-1} 2.62 kPa^{-1}	5000 cycles	218
rGO/PDMS	107 μs	20–20 000 Hz	8699	>10 000 cycles	46
Graphene-based	0.126 s	—	Gauge factor (tension): 73 Gauge factor (compression): 43	1000 cycles	219
2D MOF	5 ms	20–330 Hz	0.95 V Pa^{-1}	—	220

materials due to their high stability in air and moisture. Furthermore, the reduction of dimensionality of perovskite has also improved the piezoelectric property of the perovskite.[209] Guo *et al.* demonstrated the 2D halide perovskite as an acoustic sensor, detecting ultrasound with excellent transmission efficiency as high as 12% (Fig. 9a).[210]

Besides, traditional artificial throat sensors are usually made of graphene-based materials such as laser-induced graphene.[211,212] However, graphene-based artificial throat shows limited biocompatibility, sensitivity, accuracy and conductivity.[213,214] Therefore, other 2D materials are studied to solve these issues. Jin *et al.* reported a MXene-based piezoresistive artificial throat with a speech recognition accuracy as high as ~89%.[215] Chen *et al.* demonstrated MoS_2-based piezoelectric artificial throat (Fig. 9b), with a speech recognition accuracy of ~97%.[216]

However, the key issue faced by 2D material-based acoustic sensors is achieving the necessary sensitivity across a broad range of frequencies, especially low-frequency sounds, which are critical for applications such as speech recognition or environmental monitoring. Additionally, 2D material-based acoustic sensors face time-lag response due to the slow mechanical and electrical coupling between the sensor material and the acoustic waves. The inherent mass and stiffness of 2D materials such as graphene and TMDs can limit the speed at which the sensor responds to sound vibrations, particularly in low-frequency ranges. Moreover, signal processing delays can occur when extracting acoustic information from the sensor's analogue signals.

4.4 Olfactory

Gas sensor, also known as electronic nose, is a typical artificial olfactory device. Of the various types of gas sensors, the chemiresistive gas sensor is a commonly used sensor due to its high degree of simplicity in their architecture while maintaining a high degree of sensitivity. The principle of a chemiresistive gas sensor is detecting the change in electrical resistivity caused by the adsorption of molecules on the sensor surface,[104] leveraging the high surface-to-volume ratio and strong interaction with gas molecules of 2D materials, which allow them to act as good candidates for chemiresistive sensors.[95,104,221] Among the 2D materials, graphene is widely used due to its unparalleled combination of high sensitivity, fast responsivity, and versatility.[222–224] Table 8 summarizes the list of 2D materials used in gas sensors, comparing the key parameters against the commercial sensor.

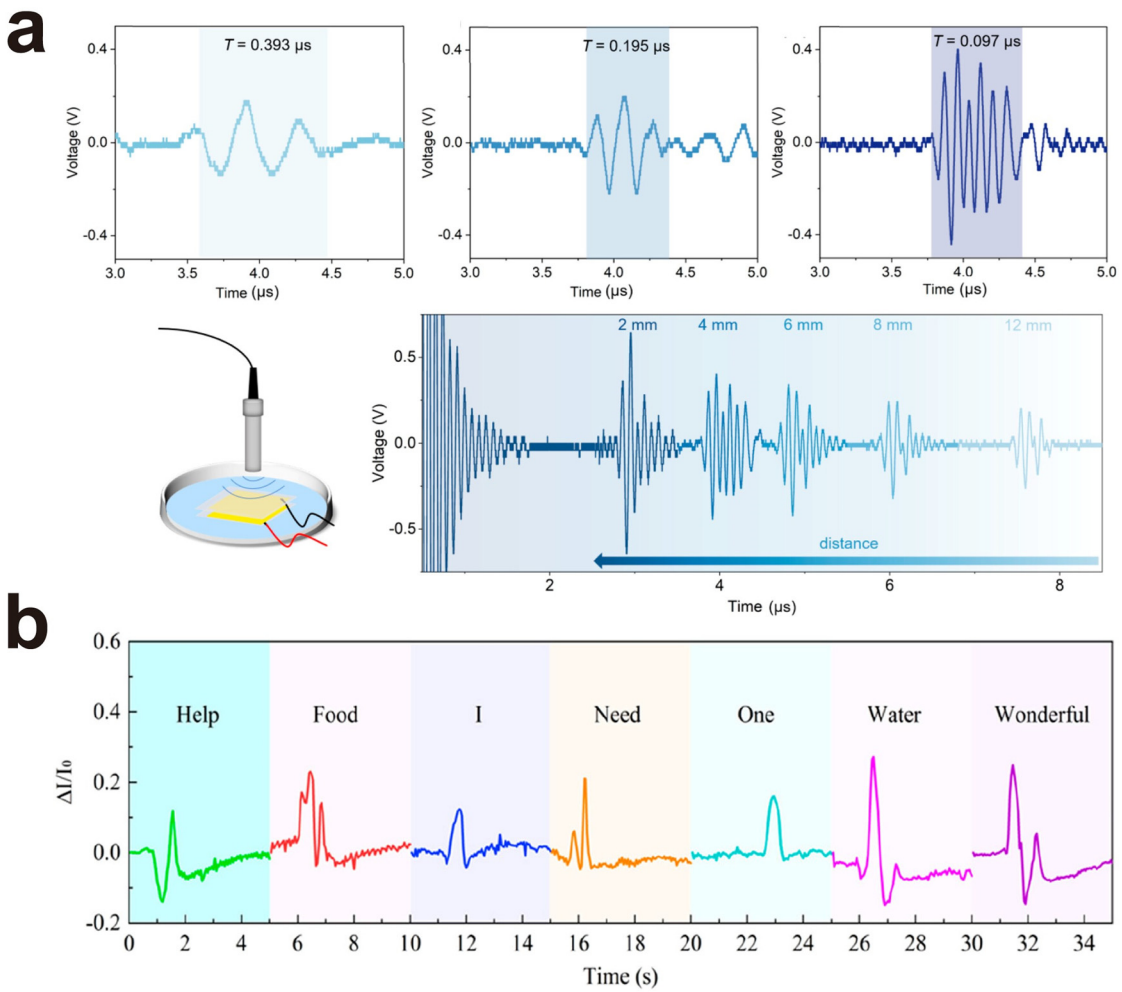

Fig. 9 2D materials for sound perception. (a) Ultrasound detection *via* a 2D perovskite-based acoustic sensor. Reproduced with permission.[210] Copyright 2023, American Chemical Society. (b) Voice recognition using a piezoelectric acoustic sensor, coupled with machine learning. Reproduced with permission.[216] Copyright 2022, American Chemical Society.

Table 8 Comparison of commercial sensors and reported 2D materials used in gas sensing

Materials	Response time	Detection range	Stability	Sensing environment	Selectivity	Ref.
Commercial sensor	—	1–50 ppm	High	—	Volatile organic compound (VOC)	https://www.winsen-sensor.com/
rGO-based	50 s	0.25% change in resistance per 1 ppm (1–10 ppm)	—	—	NH_3	244
SnO_2/rGO	—	—	H_2S: >90 days NO_2, H_2: >15 days	—	H_2S, NO_2, H_2	245
Graphene-based	~14 s	0.0579 ppm^{-1} (5–100 ppm); 0.0253 ppm^{-1} (100–200 ppm)	<1 year	H_2, air, H_2O	H_2	246
WS_2–CuO–C	37.2 s	—	25 days	100.1 °C, 500 ppb	H_2S	247
MoS_2	90–280 s	NH_3: 0.084–0.043 ppm^{-1} H_2S: 0.079–0.065 ppm^{-1}	24 weeks	—	NH_3, H_2S	248
MoS_2-based	43 s	Non-linear, 5–80 ppm	>5 weeks	80 ppm H_2 and NH_3 20 ppm NO_2 150 °C–300 °C	CO	249
WSe_2/MWCNT	32 s	10–10^5 ppb	>45 days	—	VOC	250
Black phosphorus	22 s	Down to 100 ppb	>30 days	Air, NH_3	NH_3	251
Black phosphorus–SnO_2	39.8 s	1–9 ppm	20 days	5 ppm CO_2, SO_2, NH_3, CO, C_3H_6O	H_2S	105
MXene-based	112 s	4–100 ppm	>3 weeks	Air and 100 ppm SO_2	CO, SO_2, NH_3	252
MXene/NiO	279 s	1–100 ppm	56 days	—	HCHO	253
MOF@MXene	55 s	50–400 ppb	20 days	H_2S, NO_2, SO_2, CO, NH_3, CH_4O, C_2H_6O, C_3H_6O	H_2S	254
MXene/WSe_2	9.7 s	1–40 ppm	>1 month, 40 ppm	—	VOC	255
2D MOF	1.69 min	1–100 ppm	10 days	NO_2, air	NO_2	256
2D MOF	57.3 min	50 ppb–5 ppm	—	C_7H_8, CO, CO_2, dimethyl sulfide, H_2S	H_2S	236
2D MOF	~11 s	0.1–100 ppm 3.5 ppb (limit of detection)	60 days	H_2S, NO_2, MeOH, SO_2, CO_2, CH_4, NH_3, CO	NO_2	257

Graphene-based electronic nose has been demonstrated by Kwon *et al.*, with ultrasensitive and improved selectivity to detect NO_2 by the introduction of n-dopants to graphene.[225] Naganaboina *et al.* reported graphene–CeO_2-based gas sensors for CO detection with a greater selectivity and better repeatability.[226] The performance of the sensor improved due to the presence of oxygen vacancies and the heterojunction between CeO_2 and graphene. Similarly, Tung *et al.* improved the selectivity of the graphene-based sensor using a graphene/MOF heterostructure (Fig. 10a) to detect volatile organic compounds.[227]

Besides, there has been an increase in interest in other 2D materials such as MXenes and TMDs due to graphene-based gas sensors' limitations such as low selectivity, long-term drift and long recovery time.[228,229] Zhao *et al.* reported a MXene-cationic polyacrylamide nanocomposite for flexible NH_3 gas sensing.[230] In order to improve the sensitivity of the gas sensor, Lee *et al.* developed MXene/graphene hybrid fibers for NH_3 sensing.[231] The three order higher sensitivity for these hybrid fibers were mainly attributed to the high surface-to-volume ratio. Similarly, Liu *et al.* reported a flexible and stretchable hybrid MXene/MOF aerogel gas sensor (Fig. 10b) to detect NO_2.[232] TMDs such as MoS_2 are also candidates for gas sensing. For example, functionalized MoS_2 gas sensor was demonstrated for NH_3 sensing.[233] With Au decorated on MoS_2, S vacancies were introduced, allowing higher carrier density in MoS_2, thereby enhancing the ability to detect NH_3.

Besides, 2D MOFs are a group of emerging materials that have gained attention for chemiresistive sensor applications.[234,235] The π-conjugated ligands in 2D MOFs allow effective charge delocalization. These ligands are linked to metal nodes *via* π–d hybridization, forming extended conjugation throughout the frameworks. In 2D MOFs, their porous framework structure favors the interactions between gas and materials, thus making them a highly attractive material for chemiresistive gas sensor applications. In fact, Jeon *et al.* reported a 2D MOF-based H_2S gas sensor with an improved detection limit, where the gas sensor can detect H_2S gas concentration as low as 1 ppm.[236]

Despite attracting attention due to their high sensitivity, the main issue faced by the above-mentioned 2D material-based gas sensors is their poor selectivity due to the limited variety in the adsorption sites, leading to unfavorable to selective response to gases such as H_2 and H_2S gas.[228] Moreover, when exposed to practical applications with a complex gaseous mixture, the 2D material-based gas sensors, such as graphene-based and MXenes-based gas sensors, often exhibit cross-sensitivity, responding to multiple gases. The poor selectivity often leads to false alarms and overlapping signals of gases with similar structures or functional groups. Furthermore, 2D materials such as graphene oxide exhibit a time-lag response primarily due to the slow adsorption and desorption processes of gas molecules on the material's surface, which can

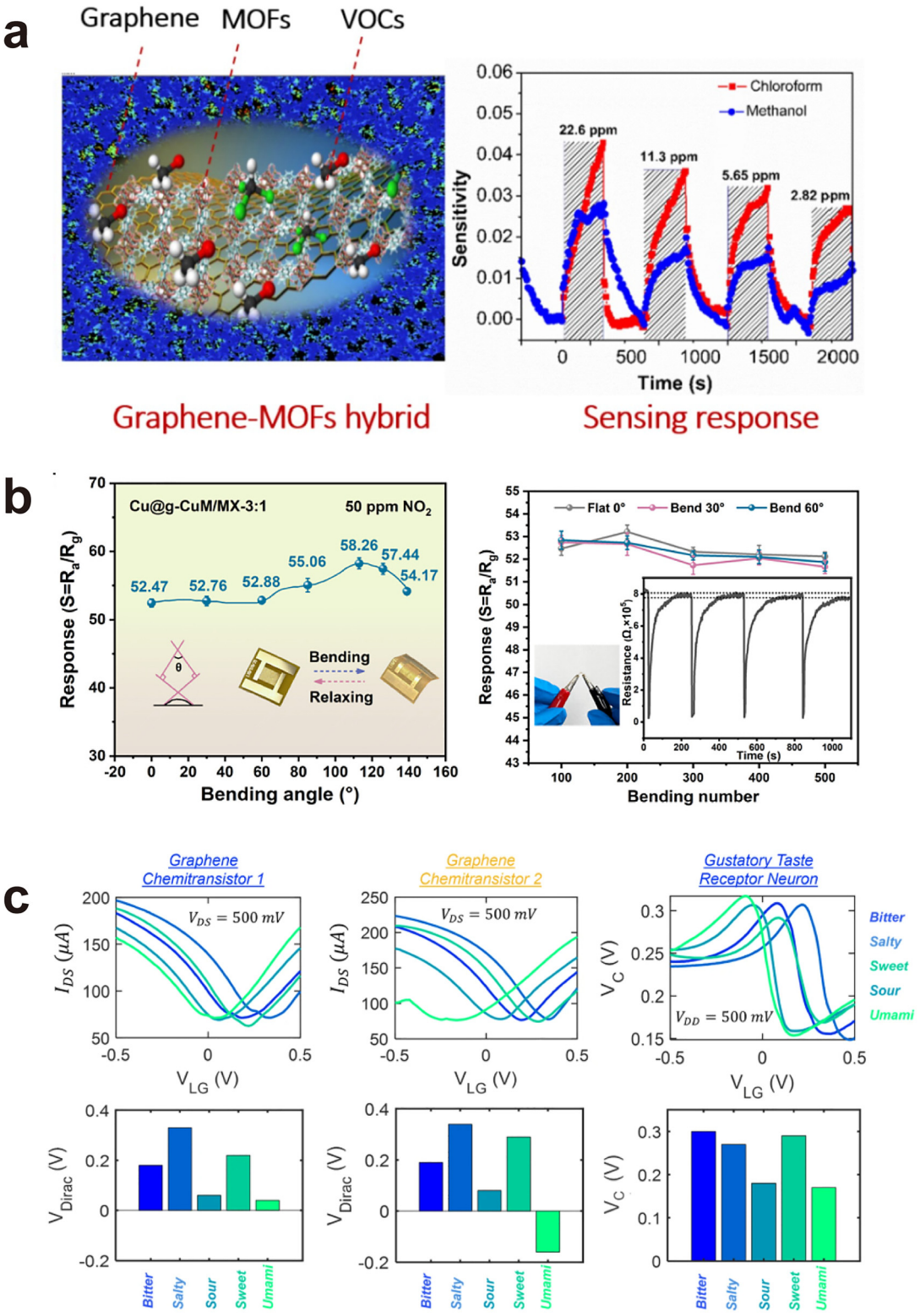

Fig. 10 2D materials for olfactory and gustatory perception. (a) Illustration of a gas sensor along with its performance to detect volatile organic compounds. Reproduced with permission.[227] Copyright 2020, Elsevier. (b) Relationship between the bending angle and the ability to detect NO_2 in a flexible gas sensor based on MXene/MOF. Reproduced with permission.[232] Copyright 2024, American Chemical Society. (c) Artificial tongue based on a graphene sensor to mimic human taste. Reproduced with permission.[259] Copyright 2023, Springer Nature.

Table 9 Comparison of the commercial sensor and reported 2D materials used in taste sensing

Materials	Response time	Detection range	Stability	Selectivity	Ref.
Commercial sensor	—	—	—	Sourness, sweetness, bitterness, astringency, umami, saltiness	https://www.insentjp.com/
MXene-based	14–22 s	—	<7 days	pH	107
AuNPs@ZIF-8/Ti_3C_2 MXene	20 min	10^{-11}–10^{-13} M	<7 days	Umami	263
Laser-induced graphene	—	1–1000 ppm	—	Sourness, sweetness, bitterness, umami, saltiness	264
Graphene-based	—	—	—	Sourness, sweetness, bitterness, umami, saltiness	259
MoS_2-based	—	10–300 μM	—	Tyramine	265
Black phosphorus	—	pH 1.0–8.0	6 days	pH	266

be detrimental to timely feedback. The electrical properties of the sensor gradually change as the gas molecules interact with the 2D material. Thus, the sensor performance degrades overtime, making their durability worse.

To address the issue of poor selectivity in gas sensors, one of the promising approaches is the functionalization of 2D materials, where noble metals such as gold, ruthenium, palladium and platinum are widely used to decorate 2D materials.[228] For example, Kim *et al.* demonstrated the tunability of the selectivity of the noble metal-decorated WS_2-based gas sensor, where Pt/Pd bimetallic nanoparticle-decorated Ru-implanted WS_2 exhibited better selectivity than pristine WS_2 and Ru-implanted WS_2.[237] Additionally, Quan *et al.* reported a fully flexible gold-decorated MXene-based gas sensor with improved selectivity (4.8% for 1 ppm) towards NO_2, which is about 3.2 and 76.0 times as high as that of the Au interdigital electrode integrated with the $Ti_3C_2T_x/WS_2$ sensor (4.8%) and the MXene electrode integrated with the $Ti_3C_2T_x$ sensor (0.2%), respectively.[238] The improvement in selectivity is due to the catalytic effect of the noble metals, promoting reactions with the targeted gas molecules, resulting in the electron transfer between gas molecules and sensing layers.[239] To overcome the issue on cross-sensitivity, assembling sensor arrays with multiple sensing units are used to detect different targeted gases. Yuan *et al.* demonstrated high selectivity for multiple-gas detection by assembling multiple gas sensing units, where each unit was decorated with specific noble metals (Ru and Ag) or silicon oxide SiO_x to enhance selectivity for targeted gases (NH_3, H_2S and H_2O, respectively).[240] However, the enhancement in the selectivity of gas sensor based on 2D materials is highly dependent on optimal conditions, such as the type, implantation dose, and quantity of decorated noble metals.

Besides the functionalization of 2D materials and sensor arrays, van der Waals heterostructures can tune the selectivity of gas sensors by controlling the stacking of 2D materials.[241,242] Such phenomenon was observed in 2D MOF-based gas sensors, where Yao *et al.* reported the use of MOF-on-MOF to modify the selectivity of the gas sensor.[243] Due to the presence of an electrically non-conductive MOF layer (Cu-TCPP), which acted as the sieving layer, on the electrically conductive MOF layer (Cu-HHTP), the selectivity of the MOF-based gas sensor was tuned from NH_3 to benzene. The change in selectivity was a result of the strong interaction between NH_3 and the sieve layer (Cu-TCPP), thus refraining NH_3 gas molecules to reach the sensing layer (Cu-HHTP).

4.5 Gustatory

Gustatory perception in soft robots is obtained through mimicking a palate sensor, commonly known as electronic tongue, which is employed to differentiate the taste through the identification of chemical compounds. When 2D materials are used in palate-mimic sensors, the fundamental mechanisms rely on ion sensing. Table 9 summarizes the list of 2D materials used in gas sensors, comparing the key parameters against the commercial sensor.

Among the 2D materials, graphene and its derivations stand out from other 2D materials as a palate sensor due to its simple, miniaturized, low cost and high performance.[222,258] Ghosh *et al.* reported a graphene-based electronic tongue (Fig. 10c) that can detect taste perception like sweetness and bitterness.[259] Yu *et al.* also reported a high-sensitivity rGO-based e-tongue that can detect and distinguish multi-flavors.[260]

However, due to the low selectivity of graphenes, there is an increasing interest towards other 2D materials. Zhi *et al.* reported a MXene-based electronic tongue with good pH-sensitivity, enabling taste perception such as sourness.[261] The scope of detection in an electronic tongue is not limited to taste perception, but extended to detect specific foods or drugs. Veeralingam *et al.* demonstrated a MoS_2-based electronic tongue that detects drugs in human saliva.[262]

Gustatory sensors remain highly unexplored due to challenges in capturing and simulating these signals and the limited pioneering research on integration to soft robots. The main issue arises from the low selectivity of these 2D material-based electronics. Hence, such sensors cannot achieve simultaneous detection and differentiation of signals in complex environments. Besides, gustatory sensors suffer from time-lag response, which is caused by the slow interaction between the target chemical molecules and the 2D material surface, as well as the delay in the subsequent electrical signal change. In the case when the sensors need to detect low concentrations of gases or chemicals, which requires a longer exposure time to accumulate sufficient molecular interactions for a detectable response.

5. Multimodal sensing, artificial intelligence-promoted soft robotics, and human–robot interaction

With the uprising of internet of things (IoT) and artificial intelligence (AI), there is an increasing demand for flexible

electronics, particularly in the field of soft robotics. Known for their deformable and flexible structures, soft robots are ideally suited for delicate handling of fragile objects, and interaction with humans or complex environments. The integration of 2D material-based sensors and actuators is critical to achieve the full potential of these robots, as 2D materials such as graphene, TMDs, borophenes, and MXenes offer the flexibility, sensitivity, and responsiveness needed for high-performance multifunctional systems.

Practical applications for 2D material-based soft robots are already beginning to emerge. In healthcare, soft robots equipped with flexible sensors can be used in minimally invasive surgeries, where precise manipulation and feedback are critical. These robots can mimic the dexterity and sensitivity of human hands, which can be used for smart collision-aware surgical robots.[267]

5.1 Multimodal device for soft robotics

To date, most sensors display single sensing ability, which have been discussed in earlier sections. However, with the increasing demand for IoT, the integration of multifunctional devices into soft robots has become a hot research topic.[268–270] In soft robotic applications, the multimodal device can be categorized as a multimodal sensor and an actuation-sensing integrated device.

5.1.1 Multimodal sensor. Integrating sensors based on 2D materials such as graphene, TMDs, MXenes, and h-BN into soft robotics enables the detection of targeted stimuli while maintaining the lightweight and adaptable nature of soft robots. However, with the increasing complexity of missions for soft robots, multifunctions are required to achieve in soft robots. The integration of different devices with required functions is a solution but lowering the dexterity of the soft robots due to the heavy wiring (especially between operation and processing parts in a soft robot) to power the devices as well as collecting and analyzing data. Multimodal sensing often refers to the ability of a sensor to detect various stimuli from its surrounding environment simultaneously. These stimuli include optical, strain, pressure, humidity, and temperature. Hence, applying multimodal devices in soft robots can release the heavy wiring to maintain the dexterity of soft robots. Benefitting from the atomic thickness and response to multiple stimuli, 2D materials are promising to achieve this.

Deng *et al.* demonstrated a tactile sensor which can achieve multimodal sensing function in a single device using polyimide–MXene/$SrTiO_3$ hybrid aerogel (Fig. 11a),[271] where MXene played an important role in achieving the pressure sensing function through the piezoresistive effect. Meanwhile, the heterostructure of MXene/$SrTiO_3$ assisted in detecting thermoelectric and infrared radiation responses. Therefore, this device with heterostructures achieved not only the perception of tactile, but also the ability to sense temperature and differentiate shapes. Similarly, Saeidi-Javash demonstrated the potential of multimodal sensors using MXene/graphene for temperature and strain sensing.[272] With these promising results, the integration of such 2D material-based multimodal sensor onto a soft gripper opens up more opportunities to applications such as rescue missions, collaborative robots, fruit sorting, and intelligent prosthetics. Zhang *et al.* integrated a graphene-based tactile sensor on a soft gripper to classify the size and ripeness of kiwifruit.[273] With the graphene-based multimodal sensor, the soft gripper can perform nondestructive evaluation with a grading speed of $\sim$2.5 s per fruit with a high sensitivity of 23.65 kPa^{-1}, promoting a higher efficiency for fruits in cold chain logistics. This fast response and high sensitivity were attributed to the excellent electrical conductivity of graphene, which enables detectable change in resistivity even with small pressure or strain applied.[274]

Despite the above-mentioned successful attempts to multimodal sensing, some challenges still obstruct their deployment in soft robots. The primary issue is the degree of cross-coupling for each sensor unit from different stimuli. For electrical type sensors, electric signals (current, voltage, capacitance, and resistance) are analysed to determine the stimuli. Separate signals responding to different stimuli are ideal to achieve this multimodal sensing. For example, the change in resistance (piezoresistive) and open-circuit voltage (thermoelectric) from MXenes represents the signals triggered by external forces and temperature, respectively, in a low cross-coupling manner.[271] In addition, such concern can be mitigated by proper encapsulation and device design of sensor, improving the accuracy.[275] A pressure and temperature all-resistive dual-mode sensor based on MXenes without crosstalk in multiple states was reported, which was achieved by simple PDMS encapsulation. A temperature-independent pressure sensor is developed by constructing a more conductive silver film on the PDMS contacted with the MXene film to form a two-phase contact mechanism with different conductivities. Furthermore, a pressure-independent temperature sensor is proposed by designing PDMS with a hollow structure around the MXene film.[276] Alternatively, machine learning is promising for the recognition of complex signals after effective training,[277] which can be a potential solution to this issue. Therefore, the integration of different active 2D materials and suitable device designs is promising to address the challenge from multimodal sensors.

5.1.2 Actuation-sensing integrated device. Other than multimodal sensors, multimodal devices such as multi-responsive actuators with self-sensing function for soft robotics also garner attention due to their ability to monitor its action in real time. By combining the actuation and sensing functions to a single device, it enables a more precisely controlled soft robot due to the real-time feedback of small deformation detected from the self-sensing function which cannot be observed visually.[171,278,279] Among the reported multimodal devices, 2D materials such as graphene and its derivatives,[279–281] and MXenes[278,282–286] are widely studied. Graphene and its derivatives (GO, rGO) are commonly used to fabricate such multimodal devices due to their multi-responsiveness arising from their hydration–dehydration behaviors, high thermal conductivity, and excellent electrical conductivity.[287–290] However, due to low infrared absorption of graphene and its derivatives, high infrared intensity is required to trigger the actuator.[291–293]

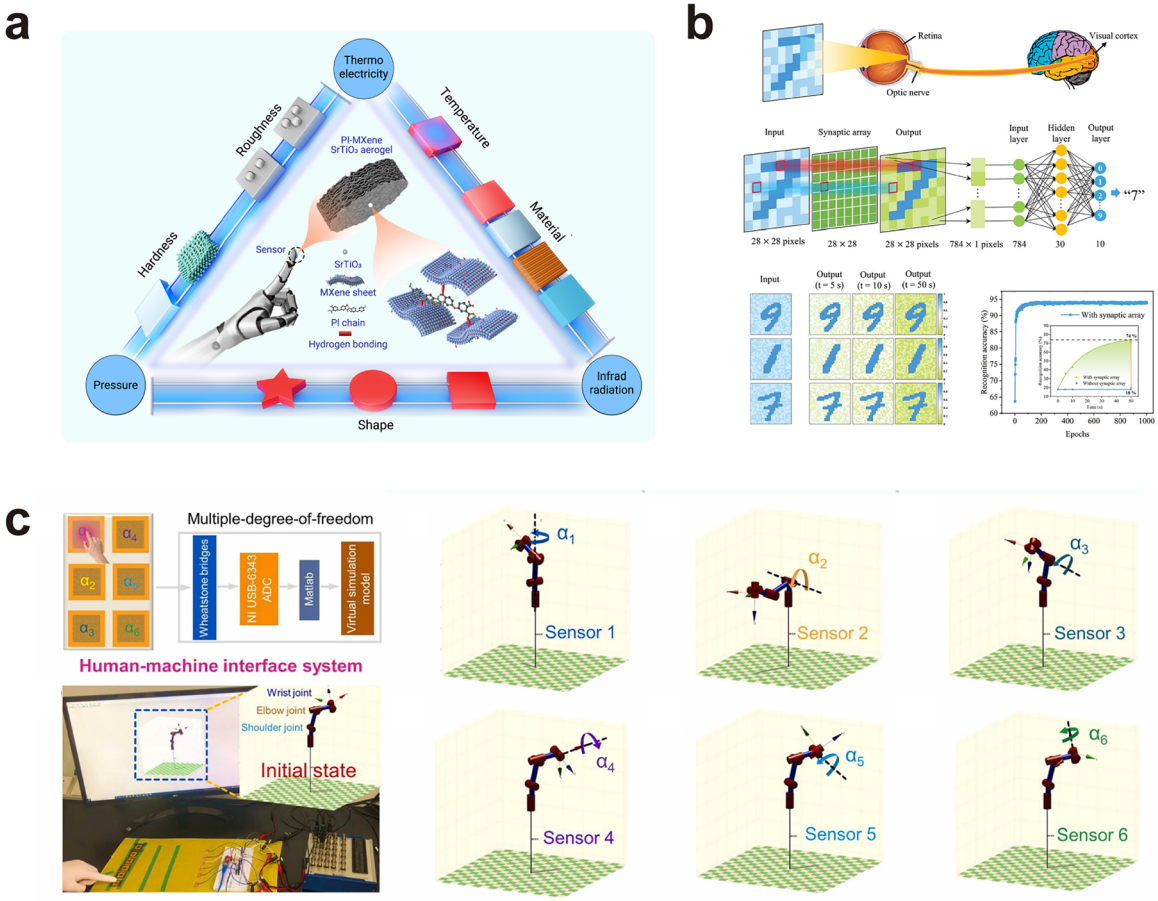

Fig. 11 Advanced applications of 2D materials in soft robotics. (a) Illustration of the stimuli of a MXene-based multimodal sensor that can simultaneously detect shape and temperature. Reproduced with permission.[271] Copyright 2024, Cell Press. (b) Illustration of artificial synapses to mimic the human visual system. Reproduced with permission.[140] Copyright 2024, John Wiley and Sons. (c) Demonstration of the potential application of the human–machine interface using a pressure sensor. Reproduced with permission.[183] Copyright 2022, Elsevier.

Moreover, graphene-based actuator mainly relies on their piezoresistive property. When the graphene-based multimodal actuator with self-sensing function is exposed to resistance-dependent stimuli, it interferes with the piezoresistive signals.[292] To overcome the challenges, attention has shifted to multi-responsive MXenes, which possess high electrical conductivity (up to 24 000 S cm^{-1}), hydration–dehydration behavior, and high photothermal conversion capability.[294–297] Zhao *et al.* demonstrated a MXene-based multi-responsive actuator with self-sensing capabilities.[283] The MXene-based multi-responsive actuator responded to stimuli such as humidity, temperature, and infrared light, where the self-sensing functions were contributed by strain-induced piezoresistive and thermoresistive MXene-based sensors. Interestingly, this piezoresistive response does not interfere with the actuation process, as the actuation process is triggered by infrared irradiation. Similarly, Zhou *et al.* reported MXene-based self-powered light-driven actuators with multimodal sensing functions, enabling the actuator to perceive non-contact temperature through photo-thermoelectric effects and tactile sensing through triboelectric effects.[284] The perceptual signals collected and converted by the actuator achieved an impressive accuracy of 98% with through training using a multilayer perceptron neural network.

5.2 Artificial intelligence promoted soft robotics

The role of AI in a soft robot is equivalent to the function of the human brain, where it has the ability to acquire knowledge, possess cognitive skills, and even develop motor. Therefore, AI usually exists in two forms in soft robotics-machine learning and artificial synapses.[298] Of these, 2D materials play a key role in the latter.

With the increasing demand for AI, memristive artificial synapses based on 2D materials have attracted intensive attention due to their unique characteristics.[299–301] Memristive artificial synapses required low power switching capability, excellent electrical and physical tuning properties and hetero-integration compatibility. Of these, 2D materials such as graphene, TMDs, and h-BN have exhibited to be emerging materials for low-power and high-performance memristive artificial synapses.[302–305] While two-terminal memristors exhibit basic synaptic function, three-terminal memristors are able to perform more complexed tasks. The degree of complication of the sensing required directly determines the type of memristors

used. Some of the synaptic functions these artificial synapses possess include short-term plasticity, long-term plasticity, short-term depression, long-term depression, spike term-dependent plasticity, and paired pulse facilitation. Some of these artificial synapses were demonstrated by Wang *et al.*, where they integrated the visual sensor with artificial synapses so as to mimic the whole human visual system (Fig. 11b).[140]

5.3 Two-dimensional material-based soft robots for human–robot interaction and healthcare

Human–robot interaction (HRI), an analogue of human–machine interface (HMI), is a system that promotes interaction between human and robots. It acts as a bridge between the end user and technology, allowing users to operate and communicate with soft robots. HRI sensor applications include electronic skin, healthcare monitoring, and intelligent recognition, of which 2D materials play a critical role in HRI ranging from sensing, processing to even a feedback loop.[306]

Some of the more common examples to demonstrate the application of HRI are pressure sensors. Hou *et al.* assembled a borophene pressure sensor with a sensitivity ranging between 0.07 kPa^{-1} and 2.16 kPa^{-1}, a detection limit of 10 Pa, and a fast response time of 90 ms.[183] The demonstration of the pressure sensor towards the application of HRI (Fig. 11c) has also been shown by connecting the pressure to a robotic arm so as to control it. Mukherjee *et al.* demonstrated a cognitive robotic gripper that can perform cognitive decision-making tasks with a graphene-based multi-array sensor,[199] graphene acts the capacitive pressure sensor with a response time of 0.3 s, which provides real-time feedback on the slippage detection thus preventing over-exertion of pressure on the targeted object.

Collaborative robot (cobot) with graphene-based electronic skin has been prototyped, demonstrating the possibility of integrating a 2D material-based tactile sensor with a robotic control system,[307] where graphene is the active material of the piezoresistive pressure sensor. However, the reaction time of the soft robot is about 0.2 s due to the measurement and computational delay. One practical application of such sensor in cobot is to avoid its collision with human and its surroundings, which can promote a safer co-workspace between human and soft robots, while boosting the production process. Similarly, Klimaszewski *et al.* demonstrated an identical function through the integration of a capacitive graphene tactile sensor onto a soft robot.[308] The reaction time of the soft robot was ~2500 ms, which might be slow for collision prevention. Despite the prolonged reaction time resulting from the filtering of undesired environmental noise, the detection quality improved, enabling the sensor to estimate and brake at a proximity distance of approximately 20 mm or less. The primary challenge is to reduce the reaction time while maintaining the precise and robust proximity distance estimation. Integrating a multimodal sensor into the cobot could address this issue by ensuring that the cobot does not rely solely on a single stimulus during the decision-making process.

In practical applications, one of the more investigated applications is in the healthcare industry such as rehabilitation and prosthetic limb feedback and/or control. William *et al.* reported the use of graphene-based composites for prosthetic upper limb feedback, whereby the prosthetic limb was able to detect pressure, temperature and movement with an accuracy of ~95% due to excellent stability of the graphene-based piezoresistive sensor.[309] Rehabilitation hand for patient suffering from stroke has also been demonstrated by Zhang *et al.*, where an rGO-based piezoresistive pressure sensor was integrated onto a prosthetic hand,[310] with a high operation range (2–1200 kPa) and a high sensitivity (6.03 kPa^{-1}). This prosthetic hand with an embedded tactile sensor can help to monitor the compression strength and duration during rehabilitation to prevent muscle atrophy and even promote recovery. Other than 2D material-based tactile sensors, optical sensors are also integrated to retinal prosthesis for rehabilitation. Choi *et al.* has demonstrated the feasibility of using MoS_2–graphene as an implantation optoelectronic device that can be used as a retinal prosthesis.[311] The MoS_2–graphene photodetector is able to detect the visible light, without capturing IR noises due to the wide bandgap of MoS_2, making it promising in soft implantable optoelectronic devices.

6. Summary and perspectives

The recent progress in the study of 2D materials is summarized in this review with a focus on their specific roles in soft robotics applications, including actuation and sensing components. The device fabrication techniques, various actuation mechanisms, different movement modes, and sensing mechanisms categorized by human–mimic perceptions (sight, taste, smell, sound and tactile) are discussed. We also highlight the advanced applications of 2D materials in soft robotics including multimodal device, AI-promoted device, and HMI. The high thermal and electrical conductivity of 2D materials, alongside the unique flexibility and conformability, have made them candidates in soft robotics field. Despite delightful progress in this research topic, some issues still obstruct the practical applications. Considering the current development of 2D materials, the challenges can be divided into three parts: (1) reliable preparation roadmap for 2D materials, including direct deposition and composite fabrication, (2) streamlined configuration, and (3) closed-loop feedback (Fig. 12).

6.1 Reliable preparation roadmap for 2D materials

Since most of the components are based on polymers in soft robotics, temperature is the primary factor that limits the preparation process. Various fabrication techniques with advantages and disadvantages for 2D materials are listed in Table 1. The shortlisted technical routes to soft robotics can be categorized to three methods: CVD plus post-transfer, low-temperature deposition, and composite fabrication *via* 2D inks comprising 2D flakes dispersed in the polymer melt or solution. Despite the ultrahigh quality of 2D films provided by CVD, the transfer process still poses challenges to get a film without crack and contamination. The weak interface between

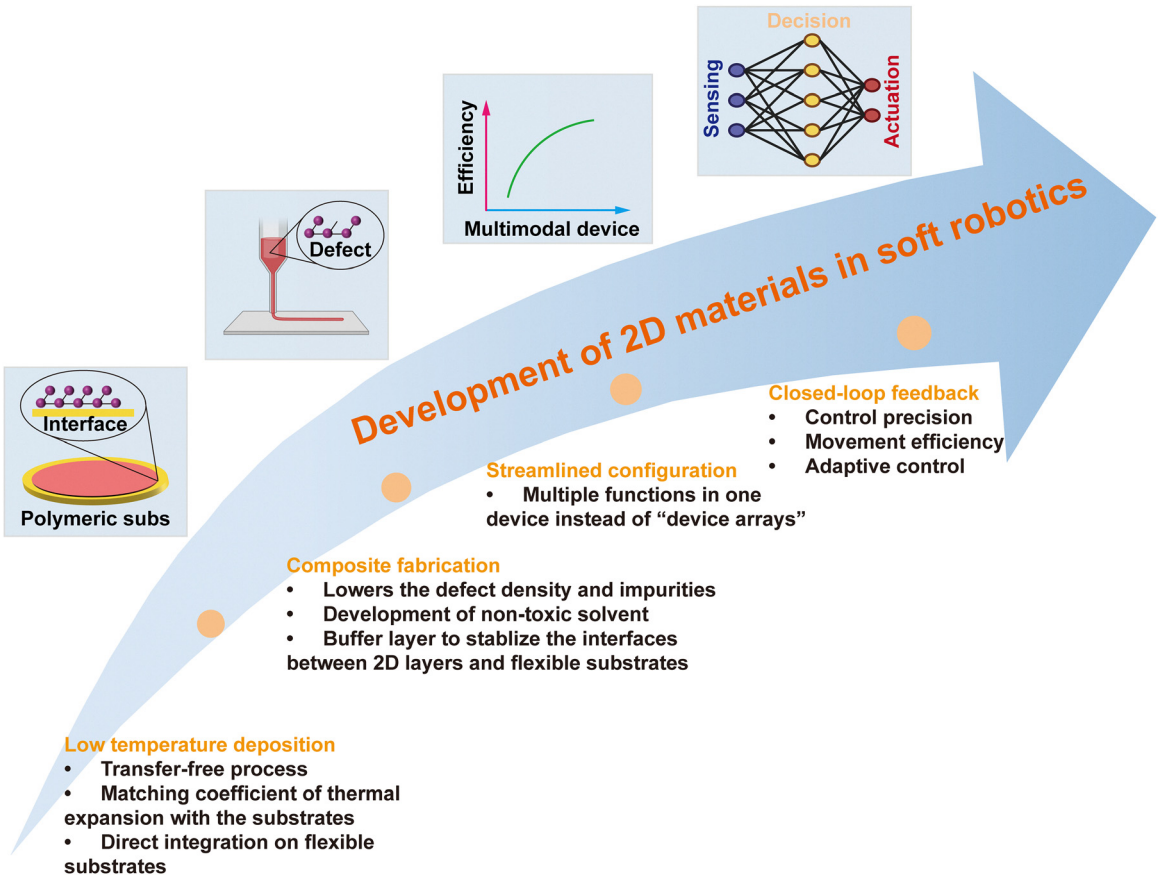

Fig. 12 Schematic depicting the development of 2D materials in soft robotics.

the 2D films with their new substrates is also detrimental to the long-term durability of the integrated devices. Therefore, more attention should be paid to the encapsulation process.

Given the multiple steps for the conventional technical route (CVD-transfer-encapsulation), low temperature deposition and composite fabrication are expected to be the alternative solutions. With a thermal process under moderate temperatures (compatible with polymers), transition interfaces between 2D films/flakes and polymeric substrates/matrix are expected to stabilize the structure, enabling higher durability and stability. It should be noted that these two technical routes can be practical only when the defect density of 2D materials is down to an acceptable level.

6.2 Streamlined configuration

The integration of multiple devices into a system to achieve desired functions has been proved successful in rigid robots. However, this significantly enhances the complexity for soft robotic systems due to the heavy external wiring. The wiring can be detrimental to the movements of soft robotics, reducing the dexterity. Therefore, the trend in integrating soft robotics is toward streamlined configuration, which involves deploying multimodal devices to reduce the total number of devices and eliminate the heavy wiring. Devices with heterostructures and multiple layers are required to achieve streamlined configuration.[18,19,312] However, the high degree of cross-coupling from different stimuli is a challenge obstructing the practical applications of multimodal sensors in soft robotics. The decoding of signals for different stimuli will be another research topic with the increasing numbers of multimodal sensors.[313]

6.3 Closed-loop feedback

The reliability of current soft robotics still cannot satisfy the commercial requirements. Next, actuators controlled by the built-in sensors or ex-site sensors will be the general route to provide real-time feedback and correction.[20,314] This offers enhanced accuracy and instantaneous response to emergency for soft actuators. The sensor with stable sensitivity is the primary factor to achieve closed-loop feedback. Second, the time lag from stimuli from an external environment to a decision made by central processor/decision maker to the reaction by the robots is too long for a timely response in a closed-loop feedback system. For example, slippage sensor with ultrafast response (below 500 ms) can be applied to detect slippage between soft grippers and objects, followed by applying a higher grasping force to the actuator. This requires fast feedback in each step, including sensing, decision making and actuation, to halt the slippage.

To solve these challenges, the development of 2D materials including material fabrication, device integration, and system establishment are indispensable. This requires multidisciplinary development and progress. A breakthrough at any

step along the technological route can approach commercial robotic applications.

Author contributions

Y. L. and J. A. O. contributed equally to this work. Y. L. and J. A. O. wrote the manuscript. P. S. L. supervised the project and reviewed the manuscript.

Conflicts of interest

The authors declare no competing interests.

Data availability

No primary research results, software or code has been included, and no new data were generated or analyzed as part of this review.

Acknowledgements

This research is supported by grants from the National Research Foundation, Prime Minister's Office, Singapore, under its Campus of Research Excellence and Technological Enterprise (CREATE) programme, Smart Grippers for Soft Robotics (SGSR).

References

1 J. Shintake, V. Cacucciolo, D. Floreano and H. Shea, *Adv. Mater.*, 2018, **30**, 1707035.
2 M. Runciman, A. Darzi and G. P. Mylonas, *Soft Robot.*, 2019, **6**, 423–443.
3 G. Li, X. Chen, F. Zhou, Y. Liang, Y. Xiao, X. Cao, Z. Zhang, M. Zhang, B. Wu, S. Yin, Y. Xu, H. Fan, Z. Chen, W. Song, W. Yang, B. Pan, J. Hou, W. Zou, S. He, X. Yang, G. Mao, Z. Jia, H. Zhou, T. Li, S. Qu, Z. Xu, Z. Huang, Y. Luo, T. Xie, J. Gu, S. Zhu and W. Yang, *Nature*, 2021, **591**, 66–71.
4 T. J. Wallin, J. Pikul and R. F. Shepherd, *Nat. Rev. Mater.*, 2018, **3**, 84–100.
5 M. Li, A. Pal, A. Aghakhani, A. Pena-Francesch and M. Sitti, *Nat. Rev. Mater.*, 2022, **7**, 235–249.
6 K. S. Novoselov, A. K. Geim, S. V. Morozov, D. Jiang, Y. Zhang, S. V. Dubonos, I. V. Grigorieva and A. A. Firsov, *Science*, 2004, **306**, 666–669.
7 W. Wu, L. Wang, Y. Li, F. Zhang, L. Lin, S. Niu, D. Chenet, X. Zhang, Y. Hao, T. F. Heinz, J. Hone and Z. L. Wang, *Nature*, 2014, **514**, 470–474.
8 K. S. Kim, S. Seo, J. Kwon, D. Lee, C. Kim, J.-E. Ryu, J. Kim, J. M. Suh, H.-G. Jung, Y. Jo, J.-C. Shin, M.-K. Song, J. Feng, H. Ahn, S. Lee, K. Cho, J. Jeon, M. Seol, J.-H. Park, S. W. Kim and J. Kim, *Nature*, 2024, **636**, 615–621.
9 L. Mennel, J. Symonowicz, S. Wachter, D. K. Polyushkin, A. J. Molina-Mendoza and T. Mueller, *Nature*, 2020, **579**, 62–66.
10 D. Kireev, S. Kutagulla, J. Hong, M. N. Wilson, M. Ramezani, D. Kuzum, J.-H. Ahn and D. Akinwande, *Nat. Rev. Mater.*, 2024, **9**, 906–922.
11 I. H. Kim, S. Choi, J. Lee, J. Jung, J. Yeo, J. T. Kim, S. Ryu, S.-K. Ahn, J. Kang, P. Poulin and S. O. Kim, *Nat. Nanotechnol.*, 2022, **17**, 1198–1205.
12 C. S. Boland, U. Khan, G. Ryan, S. Barwich, R. Charifou, A. Harvey, C. Backes, Z. Li, M. S. Ferreira, M. E. Möbius, R. J. Young and J. N. Coleman, *Science*, 2016, **354**, 1257–1260.
13 F. Xiao, S. Naficy, G. Casillas, M. H. Khan, T. Katkus, L. Jiang, H. Liu, H. Li and Z. Huang, *Adv. Mater.*, 2015, **27**, 7196–7203.
14 A. T. Hoang, L. Hu, B. J. Kim, T. T. N. Van, K. D. Park, Y. Jeong, K. Lee, S. Ji, J. Hong, A. K. Katiyar, B. Shong, K. Kim, S. Im, W. J. Chung and J.-H. Ahn, *Nat. Nanotechnol.*, 2023, **18**, 1439–1447.
15 W. Huang, Y. Zhang, M. Song, B. Wang, H. Hou, X. Hu, X. Chen and T. Zhai, *Chin. Chem. Lett.*, 2022, **33**, 2281–2290.
16 Z. Li, Y. Lv, L. Ren, J. Li, L. Kong, Y. Zeng, Q. Tao, R. Wu, H. Ma, B. Zhao, D. Wang, W. Dang, K. Chen, L. Liao, X. Duan, X. Duan and Y. Liu, *Nat. Commun.*, 2020, **11**, 1151.
17 K. Yi, Y. Wu, L. An, Y. Deng, R. Duan, J. Yang, C. Zhu, W. Gao and Z. Liu, *Adv. Mater.*, 2024, **36**, 2403494.
18 Z.-H. Tang, W.-B. Zhu, Y.-Q. Mao, Z.-C. Zhu, Y.-Q. Li, P. Huang and S.-Y. Fu, *ACS Appl. Mater. Interfaces*, 2022, **14**, 21474–21485.
19 Y. Wang, H. Wu, L. Xu, H. Zhang, Y. Yang and Z. L. Wang, *Sci. Adv.*, 2020, **6**, eabb9083.
20 L. Li, S. Li, W. Wang, J. Zhang, Y. Sun, Q. Deng, T. Zheng, J. Lu, W. Gao, M. Yang, H. Wang, Y. Pan, X. Liu, Y. Yang, J. Li and N. Huo, *Nat. Commun.*, 2024, **15**, 6261.
21 A. K. Katiyar, A. T. Hoang, D. Xu, J. Hong, B. J. Kim, S. Ji and J.-H. Ahn, *Chem. Rev.*, 2024, **124**, 318–419.
22 Y. Hou, J. Zhou, Z. He, J. Chen, M. Zhu, H. Wu and Y. Lu, *Nat. Commun.*, 2024, **15**, 4033.
23 A. Castellanos-Gomez, M. Poot, G. A. Steele, H. S. J. van der Zant, N. Agraït and G. Rubio-Bollinger, *Adv. Mater.*, 2012, **24**, 772–775.
24 J. L. Feldman, *J. Phys. Chem. Solids*, 1976, **37**, 1141–1144.
25 Y. Pang, Z. Yang, Y. Yang and T.-L. Ren, *Small*, 2020, **16**, 2070083.
26 C. Cho, Z. Zhang, J. M. Kim, P. J. Ma, M. F. Haque, P. Snapp and S. Nam, *Nano Lett.*, 2023, **23**, 9340–9346.
27 H. Jang, K. Sel, E. Kim, S. Kim, X. Yang, S. Kang, K.-H. Ha, R. Wang, Y. Rao, R. Jafari and N. Lu, *Nat. Commun.*, 2022, **13**, 6604.
28 D. Kireev, S. K. Ameri, A. Nederveld, J. Kampfe, H. Jang, N. Lu and D. Akinwande, *Nat. Protoc.*, 2021, **16**, 2395–2417.
29 W. Yan, H.-R. Fuh, Y. Lv, K.-Q. Chen, T.-Y. Tsai, Y.-R. Wu, T.-H. Shieh, K.-M. Hung, J. Li, D. Zhang, C. Ó. Coileáin, S. K. Arora, Z. Wang, Z. Jiang, C.-R. Chang and H.-C. Wu, *Nat. Commun.*, 2021, **12**, 2018.
30 P. Gant, P. Huang, D. Pérez de Lara, D. Guo, R. Frisenda and A. Castellanos-Gomez, *Mater. Today*, 2019, **27**, 8–13.

31 J. He, P. Huang, B. Li, Y. Xing, Z. Wu, T.-C. Lee and L. Liu, *Adv. Mater.*, 2025, **37**, 2413648.
32 H. Song, J. Liu, B. Liu, J. Wu, H.-M. Cheng and F. Kang, *Joule*, 2018, **2**, 442–463.
33 H. Cheng, Q. Liu, S. Han, S. Zhang, X. Ouyang, X. Wang, Z. Duan, H. Wei, X. Zhang, N. Ma and M. Xue, *ACS Appl. Mater. Interfaces*, 2020, **12**, 37637–37646.
34 K. F. Mak, C. Lee, J. Hone, J. Shan and T. F. Heinz, *Phys. Rev. Lett.*, 2010, **105**, 136805.
35 J. Wu, D. Yang, J. Liang, M. Werner, E. Ostroumov, Y. Xiao, K. Watanabe, T. Taniguchi, J. I. Dadap, D. Jones and Z. Ye, *Sci. Adv.*, 2022, **8**, eade3759.
36 Q. Tang and D.-E. Jiang, *Chem. Mater.*, 2015, **27**, 3743–3748.
37 L. H. Li, J. Cervenka, K. Watanabe, T. Taniguchi and Y. Chen, *ACS Nano*, 2014, **8**, 1457–1462.
38 L. Liu, S. Ryu, M. R. Tomasik, E. Stolyarova, N. Jung, M. S. Hybertsen, M. L. Steigerwald, L. E. Brus and G. W. Flynn, *Nano Lett.*, 2008, **8**, 1965–1970.
39 X. Wang, W. Fan, Z. Fan, W. Dai, K. Zhu, S. Hong, Y. Sun, J. Wu and K. Liu, *Nanoscale*, 2018, **10**, 3540–3546.
40 W. Zhang, K. Matsuda and Y. Miyauchi, *ACS Omega*, 2019, **4**, 10322–10327.
41 M. van Druenen, *Adv. Mater. Interfaces*, 2020, **7**, 2001102.
42 A. Iqbal, J. Hong, T. Y. Ko and C. M. Koo, *Nano Convergence*, 2021, **8**, 9.
43 X. Shen, X. Lin, Y. Peng, Y. Zhang, F. Long, Q. Han, Y. Wang and L. Han, *Nano-Micro Lett.*, 2024, **16**, 201.
44 S. Conti, G. Calabrese, K. Parvez, L. Pimpolari, F. Pieri, G. Iannaccone, C. Casiraghi and G. Fiori, *Nat. Rev. Mater.*, 2023, **8**, 651–667.
45 S. Pinilla, J. Coelho, K. Li, J. Liu and V. Nicolosi, *Nat. Rev. Mater.*, 2022, **7**, 717–735.
46 T.-S. Dinh Le, J. An, Y. Huang, Q. Vo, J. Boonruangkan, T. Tran, S.-W. Kim, G. Sun and Y.-J. Kim, *ACS Nano*, 2019, **13**, 13293–13303.
47 D. Kireev, K. Sel, B. Ibrahim, N. Kumar, A. Akbari, R. Jafari and D. Akinwande, *Nat. Nanotechnol.*, 2022, **17**, 864–870.
48 Y. J. Park, B. K. Sharma, S. M. Shinde, M.-S. Kim, B. Jang, J.-H. Kim and J.-H. Ahn, *ACS Nano*, 2019, **13**, 3023–3030.
49 J. Jang, H. Kim, S. Ji, H. J. Kim, M. S. Kang, T. S. Kim, J.-E. Won, J.-H. Lee, J. Cheon, K. Kang, W. B. Im and J.-U. Park, *Nano Lett.*, 2020, **20**, 66–74.
50 F. Bertoldo, R. R. Unocic, Y.-C. Lin, X. Sang, A. A. Puretzky, Y. Yu, D. Miakota, C. M. Rouleau, J. Schou, K. S. Thygesen, D. B. Geohegan and S. Canulescu, *ACS Nano*, 2021, **15**, 2858–2868.
51 J. K. Han, S. Kim, S. Jang, Y. R. Lim, S.-W. Kim, H. Chang, W. Song, S. S. Lee, J. Lim, K.-S. An and S. Myung, *Nano Energy*, 2019, **61**, 471–477.
52 L. Liu, T. Li, L. Ma, W. Li, S. Gao, W. Sun, R. Dong, X. Zou, D. Fan, L. Shao, C. Gu, N. Dai, Z. Yu, X. Chen, X. Tu, Y. Nie, P. Wang, J. Wang, Y. Shi and X. Wang, *Nature*, 2022, **605**, 69–75.
53 G. Liu, Z. Tian, Z. Yang, Z. Xue, M. Zhang, X. Hu, Y. Wang, Y. Yang, P. K. Chu, Y. Mei, L. Liao, W. Hu and Z. Di, *Nat. Electron.*, 2022, **5**, 275–280.
54 I. Cheliotis and I. Zergioti, *2D Mater.*, 2024, **11**, 022004.
55 T. Jurca, M. J. Moody, A. Henning, J. D. Emery, B. Wang, J. M. Tan, T. L. Lohr, L. J. Lauhon and T. J. Marks, *Angew. Chem., Int. Ed.*, 2017, **56**, 4991–4995.
56 F. Liu, W. Wu, Y. Bai, S. H. Chae, Q. Li, J. Wang, J. Hone and X. Y. Zhu, *Science*, 2020, **367**, 903–906.
57 D. Gupta, V. Chauhan and R. Kumar, *Inorg. Chem. Commun.*, 2022, **144**, 109848.
58 X.-W. Lu, Z. Li, C.-K. Yang, W. Mou and L. Jiao, *Nano Res.*, 2024, **17**, 3217–3223.
59 Y. Li, R. Goei, A. Jiamin Ong, Y. Zou, A. Shpatz Dayan, S. Rahmany, L. Etgar and A. Iing Yoong Tok, *Mater. Today Energy*, 2024, **39**, 101457.
60 X. Xu, T. Guo, H. Kim, M. K. Hota, R. S. Alsaadi, M. Lanza, X. Zhang and H. N. Alshareef, *Adv. Mater.*, 2022, **34**, 2108258.
61 M. Mariello, L. Fachechi, F. Guido and M. De Vittorio, *Adv. Funct. Mater.*, 2021, **31**, 2101047.
62 Y. Zhang, D. Wen, M. Liu, Y. Li, Y. Lin, K. Cao, F. Yang and R. Chen, *Adv. Mater. Interfaces*, 2022, **9**, 2101857.
63 K. Shrestha, G. B. Pradhan, M. Asaduzzaman, M. S. Reza, T. Bhatta, H. Kim, Y. Lee and J. Y. Park, *Adv. Energy Mater.*, 2024, **14**, 2302471.
64 H. Qin, V. Sorkin, Q.-X. Pei, Y. Liu and Y.-W. Zhang, *J. Appl. Mech.*, 2020, **87**, 030802.
65 K. Chae, V. T. Nguyen, S. Lee, T. Q. Phung, Y. Sim, M.-J. Seong, S. W. Lee, Y. H. Ahn, S. Lee, S. Ryu and J.-Y. Park, *Appl. Surf. Sci.*, 2022, **605**, 154736.
66 M. W. M. Tan, H. Wang, D. Gao, P. Huang and P. S. Lee, *Chem. Soc. Rev.*, 2024, **53**, 3485–3535.
67 Y. Jung, K. Kwon, J. Lee and S. H. Ko, *Nat. Commun.*, 2024, **15**, 3510.
68 X. Chen, I. M. Kislyakov, T. Wang, Y. Xie, Y. Wang, L. Zhang and J. Wang, *Nat. Commun.*, 2023, **14**, 2135.
69 X. Huang, X. Xiang, C. Li, J. Nie, Y. Shao, Z. Xu and Q. Zheng, *Nat. Commun.*, 2025, **16**, 493.
70 S. K. Srivastava, M. Medina-Sánchez, B. Koch and O. G. Schmidt, *Adv. Mater.*, 2016, **28**, 832–837.
71 W. Gao and J. Wang, *ACS Nano*, 2014, **8**, 3170–3180.
72 B. Khezri, S. M. Beladi Mousavi, L. Krejčová, Z. Heger, Z. Sofer and M. Pumera, *Adv. Funct. Mater.*, 2019, **29**, 1806696.
73 L. Breuer, J. Pilas, E. Guthmann, M. J. Schöning, R. Thoelen and T. Wagner, *Sens. Actuators, B*, 2019, **288**, 579–585.
74 M. F. Reynolds and M. Z. Miskin, *MRS Bull.*, 2024, **49**, 107–114.
75 B. Sharma and A. Sharma, *Adv. Eng. Mater.*, 2022, **24**, 2100738.
76 J. Fu, Y. Li, T. Zhou, S. Fang, M. Zhang, Y. Wang, K. Li, W. Lian, L. Wei, R. H. Baughman and Q. Cheng, *Sci. Adv.*, 2025, **11**, eadt1560.
77 S. Chen, S. F. Tan, H. Singh, L. Liu, M. Etienne and P. S. Lee, *Adv. Mater.*, 2024, **36**, 2307045.
78 Y. Roh, Y. Lee, D. Lim, D. Gong, S. Hwang, M. Kang, D. Kim, J. Cho, G. Kwon, D. Kang, S. Han and S. H. Ko, *Adv. Funct. Mater.*, 2024, **34**, 2306079.

79 J. Li, K. Yu, G. Wang, W. Gu, Z. Xia, X. Zhou and Z. Liu, *Adv. Funct. Mater.*, 2023, **33**, 2300156.
80 G. Cai, J.-H. Ciou, Y. Liu, Y. Jiang and P. S. Lee, *Sci. Adv.*, 2019, **5**, eaaw7956.
81 L. Xu, F. Xue, H. Zheng, Q. Ji, C. Qiu, Z. Chen, X. Zhao, P. Li, Y. Hu, Q. Peng and X. He, *Nano Energy*, 2022, **103**, 107848.
82 D. Ren, C. Zhao, S. Zhang, K. Zhang and F. Huang, *Adv. Funct. Mater.*, 2023, **33**, 2300517.
83 J. Park, Y. Kim, H. Bark and P. S. Lee, *Small Struct.*, 2024, **5**, 2300520.
84 C. Tawk and G. Alici, *Adv. Intell. Syst.*, 2021, **3**, 2000223.
85 C. De Pascali, G. A. Naselli, S. Palagi, R. B. N. Scharff and B. Mazzolai, *Sci. Rob.*, 2022, **7**, eabn4155.
86 S. Umrao, R. Tabassian, J. Kim, V. H. Nguyen, Q. Zhou, S. Nam and I.-K. Oh, *Sci. Rob.*, 2019, **4**, eaaw7797.
87 D. Wang, Z. Chen, M. Li, Z. Hou, C. Zhan, Q. Zheng, D. Wang, X. Wang, M. Cheng, W. Hu, B. Dong, F. Shi and M. Sitti, *Nat. Commun.*, 2023, **14**, 5070.
88 L. Zong, M. Li and C. Li, *Adv. Mater.*, 2017, **29**, 1604691.
89 S. Wang, Y. Gao, A. Wei, P. Xiao, Y. Liang, W. Lu, C. Chen, C. Zhang, G. Yang, H. Yao and T. Chen, *Nat. Commun.*, 2020, **11**, 4359.
90 Y. Pang, X. Xu, S. Chen, Y. Fang, X. Shi, Y. Deng, Z.-L. Wang and C. Cao, *Nano Energy*, 2022, **96**, 107137.
91 J. Xiong, J. Chen and P. S. Lee, *Adv. Mater.*, 2021, **33**, 2002640.
92 M. Zhu, S. Biswas, S. I. Dinulescu, N. Kastor, E. W. Hawkes and Y. Visell, *Proc. IEEE*, 2022, **110**, 246–272.
93 N. R. Glavin, R. Rao, V. Varshney, E. Bianco, A. Apte, A. Roy, E. Ringe and P. M. Ajayan, *Adv. Mater.*, 2020, **32**, 1904302.
94 Z. Meng, R. M. Stolz, L. Mendecki and K. A. Mirica, *Chem. Rev.*, 2019, **119**, 478–598.
95 P. Wu, Y. Li, A. Yang, X. Tan, J. Chu, Y. Zhang, Y. Yan, J. Tang, H. Yuan and X. Zhang, *ACS Sens.*, 2024, **9**, 2728–2776.
96 J. Curie and P. Curie, *Bull. Mineral.*, 1880, **3**, 90–93.
97 Y. H. Jung, S. K. Hong, H. S. Wang, J. H. Han, T. X. Pham, H. Park, J. Kim, S. Kang, C. D. Yoo and K. J. Lee, *Adv. Mater.*, 2020, **32**, 1904020.
98 J. Zhang, H. Yao, J. Mo, S. Chen, Y. Xie, S. Ma, R. Chen, T. Luo, W. Ling and L. Qin, *Nat. Commun.*, 2022, **13**, 5076.
99 Y. Pang, H. Tian, L. Tao, Y. Li, X. Wang, N. Deng, Y. Yang and T.-L. Ren, *ACS Appl. Mater. Interfaces*, 2016, **8**, 26458–26462.
100 F.-R. Fan, Z.-Q. Tian and Z. L. Wang, *Nano Energy*, 2012, **1**, 328–334.
101 Y. Liu, J. Ping and Y. Ying, *Adv. Funct. Mater.*, 2021, **31**, 2009994.
102 M. S. Rasel, P. Maharjan, M. Salauddin, M. T. Rahman, H. O. Cho, J. W. Kim and J. Y. Park, *Nano Energy*, 2018, **49**, 603–613.
103 X. Wang, H. Zhang, L. Dong, X. Han, W. Du, J. Zhai, C. Pan and Z. L. Wang, *Adv. Mater.*, 2016, **28**, 2896–2903.
104 A. Parichenko, S. Huang, J. Pang, B. Ibarlucea and G. Cuniberti, *TrAC, Trends Anal. Chem.*, 2023, 117185.
105 Y. Zhou, Z. Hu, H. Zhao, Y. Wang, J. Li and C. Zou, *Anal. Chim. Acta*, 2023, **1245**, 340825.
106 M. Lakshmikanth, M. Saquib, A. U. Rathod, R. Nayak and M. Selvakumar, *IEEE Sens. J.*, 2025, **25**, 8008–8015.
107 H. J. Kim, C. W. Lee, S. Park, S. Choi, S. H. Park, G. B. Nam, J.-E. Ryu, T. H. Eom, B. Kim, C.-J. Kim, S. Y. Kim and H. W. Jang, *Sens. Actuators, B*, 2024, **409**, 135636.
108 Í. A. Costa, M. A. Gross, E. D. O. Alves, F. J. Fonseca and L. G. Paterno, *J. Electroanal. Chem.*, 2022, **922**, 116719.
109 L. Qian, Y. Sun, M. Wu, C. Li, D. Xie, L. Ding and G. Shi, *Nanoscale*, 2018, **10**, 6837–6843.
110 C. Ma, Y. Shi, W. Hu, M.-H. Chiu, Z. Liu, A. Bera, F. Li, H. Wang, L.-J. Li and T. Wu, *Adv. Mater.*, 2016, **28**, 3683–3689.
111 L. Tao, Z. Chen, X. Li, K. Yan and J.-B. Xu, *npj 2D Mater. Appl.*, 2017, **1**, 19.
112 A. Dodda, D. Jayachandran, A. Pannone, N. Trainor, S. P. Stepanoff, M. A. Steves, S. S. Radhakrishnan, S. Bachu, C. W. Ordonez, J. R. Shallenberger, J. M. Redwing, K. L. Knappenberger, D. E. Wolfe and S. Das, *Nat. Mater.*, 2022, **21**, 1379–1387.
113 S. Wei, F. Wang, X. Zou, L. Wang, C. Liu, X. Liu, W. Hu, Z. Fan, J. C. Ho and L. Liao, *Adv. Mater.*, 2020, **32**, 1907527.
114 H. Tian, Q. Liu, A. Hu, X. He, Z. Hu and X. Guo, *Opt. Express*, 2018, **26**, 5408–5415.
115 Z. Chen, Z. Cheng, J. Wang, X. Wan, C. Shu, H. K. Tsang, H. P. Ho and J.-B. Xu, *Adv. Opt. Mater.*, 2015, **3**, 1207–1214.
116 B. Son, Y. Wang, M. Luo, K. Lu, Y. Kim, H.-J. Joo, Y. Yi, C. Wang, Q. J. Wang, S. H. Chae and D. Nam, *Nano Lett.*, 2022, **22**, 9516–9522.
117 Y. Zhang, K. Ma, C. Zhao, W. Hong, C. Nie, Z.-J. Qiu and S. Wang, *ACS Nano*, 2021, **15**, 4405–4415.
118 Y. Zhu, Y. Wang, X. Pang, Y. Jiang, X. Liu, Q. Li, Z. Wang, C. Liu, W. Hu and P. Zhou, *Nat. Commun.*, 2024, **15**, 6015.
119 M. Dai, X. Zhang, Y. Hu, W. Chen, C. Wang, Y. Luo and Q. J. Wang, *Adv. Funct. Mater.*, 2025, 2501467.
120 T. Ji, H. Zhang, J. Guo, Y. Wang, L. Shi, Y. Wu, W. Wang, G. Li, R. Wen, L. Xiao, Q. Su, B. Xu, H. Chen and Y. Cui, *Adv. Funct. Mater.*, 2023, **33**, 2210548.
121 N. Li, S. Zhang, Y. Peng, X. Li, Y. Zhang, C. He and G. Zhang, *Adv. Funct. Mater.*, 2023, **33**, 2305589.
122 T. Tan, X. Jiang, C. Wang, B. Yao and H. Zhang, *Adv. Sci.*, 2020, **7**, 2000058.
123 Z. Cheng, R. Cao, K. Wei, Y. Yao, X. Liu, J. Kang, J. Dong, Z. Shi, H. Zhang and X. Zhang, *Adv. Sci.*, 2021, **8**, 2003834.
124 J. An, X. Zhao, Y. Zhang, M. Liu, J. Yuan, X. Sun, Z. Zhang, B. Wang, S. Li and D. Li, *Adv. Funct. Mater.*, 2022, **32**, 2110119.
125 O. Lopez-Sanchez, D. Lembke, M. Kayci, A. Radenovic and A. Kis, *Nat. Nanotechnol.*, 2013, **8**, 497–501.
126 C. K. Liu, V. Piradi, J. Song, Z. Wang, L. W. Wong, E. H. L. Tan, J. Zhao, X. Zhu and F. Yan, *Adv. Mater.*, 2022, **34**, 2204140.
127 Y. Pan, H. Wang, X. Li, X. Zhang, F. Liu, M. Peng, Z. Shi, C. Li, H. Zhang and Z. Weng, *J. Mater. Chem. C*, 2020, **8**, 3359–3366.

128 Y. Zheng, Y. Wang, Z. Li, Z. Yuan, S. Guo, Z. Lou, W. Han, G. Shen and L. Wang, *Matter*, 2023, **6**, 506–520.
129 F. Xia, T. Mueller, Y.-M. Lin, A. Valdes-Garcia and P. Avouris, *Nat. Nanotechnol.*, 2009, **4**, 839–843.
130 Y. Gao, H. K. Tsang and C. Shu, *Nanoscale*, 2018, **10**, 21851–21856.
131 C.-H. Liu, Y.-C. Chang, T. B. Norris and Z. Zhong, *Nat. Nanotechnol.*, 2014, **9**, 273–278.
132 M. Xu, S. H. Wang, B. Liu, X. M. Dong, M. N. Yu, K. L. Wang, D. Y. Zhu, X. J. Li, H. C. Sun and F. Zhang, *Adv. Mater. Technol.*, 2025, **10**, 2401700.
133 J. Liang, X. Yu, C. Cheng, B. Huang, Z. Wang and L. Huang, *J. Mater. Chem. C*, 2024, **12**, 14955–14963.
134 U. K. Aryal, M. Ahmadpour, V. Turkovic, H.-G. Rubahn, A. Di Carlo and M. Madsen, *Nano Energy*, 2022, **94**, 106833.
135 Z. Tan, Y. Wu, H. Hong, J. Yin, J. Zhang, L. Lin, M. Wang, X. Sun, L. Sun and Y. Huang, *J. Am. Chem. Soc.*, 2016, **138**, 16612–16615.
136 H. Wang, L. Li, J. Ma, J. Li and D. Li, *J. Mater. Chem. C*, 2021, **9**, 11085–11090.
137 H. P. Wang, S. Li, X. Liu, Z. Shi, X. Fang and J. H. He, *Adv. Mater.*, 2021, **33**, 2003309.
138 T. Wang, D. Zheng, K. Vegso, N. Mrkyvkova, P. Siffalovic, X. Yuan, M. G. Somekh, L. Coolen, T. Pauporte and F. Fu, *Nano Energy*, 2023, **116**, 108827.
139 B. Kim and S. I. Seok, *Energy Environ. Sci.*, 2020, **13**, 805–820.
140 Y. Wang, Y. Zha, C. Bao, F. Hu, Y. Di, C. Liu, F. Xing, X. Xu, X. Wen and Z. Gan, *Adv. Mater.*, 2024, **36**, 2311524.
141 X. Huang, Q. Li, W. Shi, K. Liu, Y. Zhang, Y. Liu, X. Wei, Z. Zhao, Y. Guo and Y. Liu, *Small*, 2021, **17**, 2102820.
142 H. Tian, X. Wang, F. Wu, Y. Yang and T. L. Ren, 2018 IEEE International Electron Devices Meeting (IEDM), San Francisco, CA, USA, 2018, pp. 38.6.1–38.6.4.
143 Y. Zou, Z. Zhang, J. Yan, L. Lin, G. Huang, Y. Tan, Z. You and P. Li, *Nat. Commun.*, 2022, **13**, 4372.
144 H. Wu, Z. Lin, J. Liu, C. Zhang, C. Tan and Z. Wang, *ACS Appl. Mater. Interfaces*, 2025, **17**, 20116–20124.
145 K. Y. Thai, I. Park, B. J. Kim, A. T. Hoang, Y. Na, C. U. Park, Y. Chae and J.-H. Ahn, *ACS Nano*, 2021, **15**, 12836–12846.
146 C. Wang, H. Nan, Q. Wu, W. Wang, T. Zheng, Z. Ni, Z. Wu, X. Wan, Z. Cai, X. Gu and S. Xiao, *ACS Appl. Mater. Interfaces*, 2025, **17**, 30019–30028.
147 S. Hong, N. Zagni, S. Choo, N. Liu, S. Baek, A. Bala, H. Yoo, B. H. Kang, H. J. Kim, H. J. Yun, M. A. Alam and S. Kim, *Nat. Commun.*, 2021, **12**, 3559.
148 D. Tan, Z. Zhang, H. Shi, N. Sun, Q. Li, S. Bi, J. Huang, Y. Liu, Q. Guo and C. Jiang, *Adv. Mater.*, 2024, **36**, 2407751.
149 Y. Zhu, C. Geng, L. Hu, L. Liu, Y. Zhu, Y. Yao, C. Li, Y. Ma, G. Li and Y. Chen, *Chem. Mater.*, 2023, **35**, 2114–2124.
150 R. M. Ansari, A. Yadav, S. Singh, B. Irziqat, C. Aivalioti, R. Zhou, M. Abulikemu, A. Azam, S. Fatayer and S. Ahmad, *ACS Mater. Lett.*, 2025, 2115–2124, DOI: **10.1021/acsmaterialslett.4c02691,**.
151 D. Kumar, H. Li, U. K. Das, A. M. Syed and N. El-Atab, *Adv. Mater.*, 2023, **35**, 2300446.
152 W. Huang, Y. Yang and H. Zhang, *Acc. Chem. Res.*, 2024, **57**, 2464–2475.
153 S. Seo, S.-H. Jo, S. Kim, J. Shim, S. Oh, J.-H. Kim, K. Heo, J.-W. Choi, C. Choi and S. Oh, *Nat. Commun.*, 2018, **9**, 5106.
154 E. O. Polat, G. Mercier, I. Nikitskiy, E. Puma, T. Galan, S. Gupta, M. Montagut, J. J. Piqueras, M. Bouwens and T. Durduran, *Sci. Adv.*, 2019, **5**, eaaw7846.
155 K. Xia, W. Wu, M. Zhu, X. Shen, Z. Yin, H. Wang, S. Li, M. Zhang, H. Wang and H. Lu, *Sci. Bull.*, 2020, **65**, 343–349.
156 Y. Wang, Z. Nie and F. Wang, *Light: Sci. Appl.*, 2020, **9**, 192.
157 D. W. Kidd, D. K. Zhang and K. Varga, *Phys. Rev. B*, 2016, **93**, 125423.
158 Z. Jiang, Z. Liu, Y. Li and W. Duan, *Phys. Rev. Lett.*, 2017, **118**, 266401.
159 A. N. Rudenko and M. I. Katsnelson, *Phys. Rev. B:Condens. Matter Mater. Phys.*, 2014, **89**, 201408.
160 P. Schmidt, F. Vialla, S. Latini, M. Massicotte, K.-J. Tielrooij, S. Mastel, G. Navickaite, M. Danovich, D. A. Ruiz-Tijerina, C. Yelgel, V. Fal'ko, K. S. Thygesen, R. Hillenbrand and F. H. L. Koppens, *Nat. Nanotechnol.*, 2018, **13**, 1035–1041.
161 S. H. Mir, V. K. Yadav and J. K. Singh, *ACS Omega*, 2020, **5**, 14203–14211.
162 G. W. Ludwig and R. L. Watters, *Phys. Rev.*, 1956, **101**, 1699–1701.
163 M. G. Mohamed, C.-C. Lee, A. F. M. El-Mahdy, J. Lüder, M.-H. Yu, Z. Li, Z. Zhu, C.-C. Chueh and S.-W. Kuo, *J. Mater. Chem. A*, 2020, **8**, 11448–11459.
164 I. C. Smith, E. T. Hoke, D. Solis-Ibarra, M. D. McGehee and H. I. Karunadasa, *Angew. Chem., Int. Ed.*, 2014, **53**, 11232–11235.
165 C. Katan, N. Mercier and J. Even, *Chem. Rev.*, 2019, **119**, 3140–3192.
166 R. L. Milot, R. J. Sutton, G. E. Eperon, A. A. Haghighirad, J. Martinez Hardigree, L. Miranda, H. J. Snaith, M. B. Johnston and L. M. Herz, *Nano Lett.*, 2016, **16**, 7001–7007.
167 F. Li, T. Shen, C. Wang, Y. Zhang, J. Qi and H. Zhang, *Nano-Micro Lett.*, 2020, **12**, 1–44.
168 W. Jiang, D. Niu, H. Liu, C. Wang, T. Zhao, L. Yin, Y. Shi, B. Chen, Y. Ding and B. Lu, *Adv. Funct. Mater.*, 2014, **24**, 7598–7604.
169 D. Niu, W. Jiang, G. Ye, K. Wang, L. Yin, Y. Shi, B. Chen, F. Luo and H. Liu, *Mater. Res. Bull.*, 2018, **102**, 92–99.
170 N. Luo, Y. Huang, J. Liu, S. C. Chen, C. P. Wong and N. Zhao, *Adv. Mater.*, 2017, **29**, 1702675.
171 Q. Ji, Z. Jing, J. Shen, Y. Hu, L. Chang, L. Lu, M. Liu, J. Liu and Y. Wu, *Adv. Intell. Syst.*, 2021, **3**, 2000240.
172 M. Tannarana, G. Solanki, S. A. Bhakhar, K. D. Patel, V. Pathak and P. M. Pataniya, *ACS Sustainable Chem. Eng.*, 2020, **8**, 7741–7749.
173 Y.-W. Cai, X.-N. Zhang, G.-G. Wang, G.-Z. Li, D.-Q. Zhao, N. Sun, F. Li, H.-Y. Zhang, J.-C. Han and Y. Yang, *Nano Energy*, 2021, **81**, 105663.
174 B. Jia, Z. Li, T. Zheng, J. Wang, Z.-J. Zhao, L. Zhao, B. Wang, J. Lu, K. Zhao, G. Luo, M. Li, Q. Lin and Z. Jiang, *Chem. Eng. J.*, 2024, **485**, 149750.

175 P. Zhang, W. Wang, Y. Ma, H. Zhang, D. Zhou, X. Ji, W. Liu, Y. Liu and D. Zhang, *Chem. Eng. J.*, 2024, **499**, 156173.
176 X. Fu, L. Zhao, Z. Yuan, Y. Zheng, V. Shulga, W. Han and L. Wang, *Adv. Mater. Technol.*, 2022, **7**, 2101511.
177 V. Adepu, C. Yoo, Y. Jung and P. Sahatiya, *Appl. Phys. Lett.*, 2023, **122**, 263505.
178 L.-J. Ji, C. Zhao, T.-Y. Yang, H.-R. Yang, M. Azeem, Z.-Y. Li, R. Feng, G.-Q. Feng, S. Li and W. Li, *APL Mater.*, 2024, **12**, 091116.
179 T. Yang, H. Xiang, C. Qin, Y. Liu, X. Zhao, H. Liu, H. Li, M. Ouzounian, G. Hong, H. Chen, Q. Dong, T. S. Hu and S. Liu, *Adv. Electron. Mater.*, 2020, **6**, 1900916.
180 P. Gajula, J. U. Yoon, I. Woo, S.-J. Oh and J. W. Bae, *Nano Energy*, 2024, **121**, 109278.
181 K. Ma, D. Su, B. Qin, J. Li, J. Zhong, C. Zhang, F. Deng, G. Shen, W. Yang, Y. Xin and X. He, *Chem. Eng. J.*, 2024, **486**, 150017.
182 Z. Yang, Q. Duan, J. Zang, Y. Zhao, W. Zheng, R. Xiao, Z. Zhang, L. Hu, G. Wu and X. Nan, *Microsyst. Nanoeng.*, 2023, **9**, 68.
183 C. Hou, G. Tai, Y. Liu, R. Liu, X. Liang, Z. Wu and Z. Wu, *Nano Energy*, 2022, **97**, 107189.
184 J. Chen, G. Ma, X. Wang, T. Song, Y. Zhu, S. Jia, X. Zhang, Y. Zhao, J. Chen, B. Yang and Y. Li, *Nanoscale*, 2024, **16**, 5999–6009.
185 J. Ji, W. Zhao, Y. Wang, Q. Li and G. Wang, *ACS Nano*, 2023, **17**, 20153–20166.
186 T. Sun, C. Yao, Z. Liu, S. Huang, X. Huang, S. Zheng, J. Liu, P. Shi, T. Zhang, H. Chen, H.-J. Chen and X. Xie, *Nano Energy*, 2024, **123**, 109395.
187 X. Tang, J. Yang, J. Luo, G. Cheng, B. Sun, Z. Zhou, P. Zhang and D. Wei, *Chem. Eng. J.*, 2024, **495**, 153281.
188 H. Zhu, Y. Wang, J. Xiao, M. Liu, S. Xiong, Z. J. Wong, Z. Ye, Y. Ye, X. Yin and X. Zhang, *Nat. Nanotechnol.*, 2015, **10**, 151–155.
189 J. H. Lee, J. Y. Park, E. B. Cho, T. Y. Kim, S. A. Han, T. H. Kim, Y. Liu, S. K. Kim, C. J. Roh and H. J. Yoon, *Adv. Mater.*, 2017, **29**, 1606667.
190 S. K. Kim, R. Bhatia, T.-H. Kim, D. Seol, J. H. Kim, H. Kim, W. Seung, Y. Kim, Y. H. Lee and S.-W. Kim, *Nano Energy*, 2016, **22**, 483–489.
191 W. Guo, Y. Xia, Y. Zhu, S. Han, Q. Li and X. Wang, *Nano Energy*, 2023, **108**, 108229.
192 Z. Chen, Z. Wang, X. Li, Y. Lin, N. Luo, M. Long, N. Zhao and J.-B. Xu, *ACS Nano*, 2017, **11**, 4507–4513.
193 J. Tan, Y. Wang, Z. Wang, X. He, Y. Liu, B. Wang, M. I. Katsnelson and S. Yuan, *Nano Energy*, 2019, **65**, 104058.
194 S. Heo, D. Y. Lee, D. Lee, Y. Lee, K. Kim, H.-S. Yun, M. J. Paik, T. J. Shin, H. S. Oh, T. Shin, J. Kim, S. H. Kim, S. I. Seok and M. Nazeeruddin, *Adv. Energy Mater.*, 2022, **12**, 2200181.
195 S. Zhang, Y. Xiao, H. Chen, Y. Zhang, H. Liu, C. Qu, H. Shao and Y. Xu, *ACS Appl. Mater. Interfaces*, 2023, **15**, 13802–13812.
196 S. K. Ghosh, J. Kim, M. P. Kim, S. Na, J. Cho, J. J. Kim and H. Ko, *ACS Nano*, 2022, **16**, 11415–11427.
197 Y. Wu, Y. Luo, P. K. Chu and C. Menon, *Nano Energy*, 2023, **111**, 108427.
198 L. Zhang, S. Zhang, C. Wang, Q. Zhou, H. Zhang and G.-B. Pan, *ACS Sens.*, 2021, **6**, 2630–2641.
199 T. Mukherjee and D. Gupta, *Commun. Eng.*, 2023, **2**, 57.
200 R. Umapathi, M. Rethinasabapathy, V. Kakani, H. Kim, Y. Park, H. K. Kim, G. M. Rani, H. Kim and Y. S. Huh, *Nano Energy*, 2025, 110689.
201 S. S. Rana, M. T. Rahman, M. A. Zahed, S. H. Lee, Y. Do Shin, S. Seonu, D. Kim, M. Salauddin, T. Bhatta and K. Sharstha, *Nano Energy*, 2022, **104**, 107931.
202 M. Kundu, D. Mondal, N. Bose, R. Basu and S. Das, *ACS Appl. Nano Mater.*, 2024, **7**, 1804–1814.
203 S. Nuthalapati, V. Shirhatti, V. Kedambaimoole, V. Pandi N, H. Takao, M. M. Nayak and K. Rajanna, *Sens. Actuators, A*, 2022, **334**, 113314.
204 M. Amjadi, K.-U. Kyung, I. Park and M. Sitti, *Adv. Funct. Mater.*, 2016, **26**, 1678–1698.
205 J. Qiu, X. Guo, R. Chu, S. Wang, W. Zeng, L. Qu, Y. Zhao, F. Yan and G. Xing, *ACS Appl. Mater. Interfaces*, 2019, **11**, 40716–40725.
206 X. Guo, Y. Huang, Y. Zhao, L. Mao, L. Gao, W. Pan, Y. Zhang and P. Liu, *Smart Mater. Struct.*, 2017, **26**, 095017.
207 X. Cao, J. Zhang, S. Chen, R. J. Varley and K. Pan, *Adv. Funct. Mater.*, 2020, **30**, 2003618.
208 G.-Y. Gou, X.-S. Li, J.-M. Jian, H. Tian, F. Wu, J. Ren, X.-S. Geng, J.-D. Xu, Y.-C. Qiao and Z.-Y. Yan, *Sci. Adv.*, 2022, **8**, eabn2156.
209 S. Rahmany, A. Shpatz Dayan, M. Wierzbowska, A. J. Ong, Y. Li, S. Magdassi, A. I. Y. Tok and L. Etgar, *ACS Energy Lett.*, 2024, **9**, 1527–1536.
210 T.-M. Guo, F.-F. Gao, Y.-J. Gong, Z.-G. Li, F. Wei, W. Li and X.-H. Bu, *J. Am. Chem. Soc.*, 2023, **145**, 22475–22482.
211 L.-Q. Tao, H. Tian, Y. Liu, Z.-Y. Ju, Y. Pang, Y.-Q. Chen, D.-Y. Wang, X.-G. Tian, J.-C. Yan and N.-Q. Deng, *Nat. Commun.*, 2017, **8**, 14579.
212 Z. Li, L. Huang, L. Cheng, W. Guo and R. Ye, *Small Methods*, 2024, 2400118.
213 S. Lee, D. Sasaki, D. Kim, M. Mori, T. Yokota, H. Lee, S. Park, K. Fukuda, M. Sekino and K. Matsuura, *Nat. Nanotechnol.*, 2019, **14**, 156–160.
214 Y. Wang, S. Lee, T. Yokota, H. Wang, Z. Jiang, J. Wang, M. Koizumi and T. Someya, *Sci. Adv.*, 2020, **6**, eabb7043.
215 Y. Jin, B. Wen, Z. Gu, X. Jiang, X. Shu, Z. Zeng, Y. Zhang, Z. Guo, Y. Chen and T. Zheng, *Adv. Mater. Technol.*, 2020, **5**, 2000262.
216 X. Chen, D. Zhang, H. Luan, C. Yang, W. Yan and W. Liu, *ACS Appl. Mater. Interfaces*, 2022, **15**, 2043–2053.
217 J. Chen, L. Li, W. Ran, D. Chen, L. Wang and G. Shen, *Nano Res.*, 2023, **16**, 3180–3187.
218 T. Su, N. Liu, D. Lei, L. Wang, Z. Ren, Q. Zhang, J. Su, Z. Zhang and Y. Gao, *ACS Nano*, 2022, **16**, 8461–8471.
219 Y. Long, P. He, R. Xu, T. Hayasaka, Z. Shao, J. Zhong and L. Lin, *Carbon*, 2020, **157**, 594–601.
220 K. Roy, S. Jana, Z. Mallick, S. K. Ghosh, B. Dutta, S. Sarkar, C. Sinha and D. Mandal, *Langmuir*, 2021, **37**, 7107–7117.

221 S. Y. Jeong, J. S. Kim and J. H. Lee, *Adv. Mater.*, 2020, **32**, 2002075.
222 J. Pang, S. Peng, C. Hou, H. Zhao, Y. Fan, C. Ye, N. Zhang, T. Wang, Y. Cao and W. Zhou, *ACS Sens.*, 2023, **8**, 482–514.
223 E. Singh, M. Meyyappan and H. S. Nalwa, *ACS Appl. Mater. Interfaces*, 2017, **9**, 34544–34586.
224 P. Recum and T. Hirsch, *Nanoscale Adv.*, 2024, **6**, 11–31.
225 B. Kwon, H. Bae, H. Lee, S. Kim, J. Hwang, H. Lim, J. H. Lee, K. Cho, J. Ye and S. Lee, *ACS Nano*, 2022, **16**, 2176–2187.
226 V. R. Naganaboina and S. G. Singh, *Appl. Surf. Sci.*, 2021, **563**, 150272.
227 T. T. Tung, M. T. Tran, J.-F. Feller, M. Castro, T. Van Ngo, K. Hassan, M. J. Nine and D. Losic, *Carbon*, 2020, **159**, 333–344.
228 A. Mirzaei, J.-Y. Kim, H. W. Kim and S. S. Kim, *Acc. Chem. Res.*, 2024, **57**, 2395–2413.
229 K. Yu, P. Wang, G. Lu, K.-H. Chen, Z. Bo and J. Chen, *J. Phys. Chem. Lett.*, 2011, **2**, 537–542.
230 L. Zhao, Y. Zheng, K. Wang, C. Lv, W. Wei, L. Wang and W. Han, *Adv. Mater. Technol.*, 2020, **5**, 2000248.
231 S. H. Lee, W. Eom, H. Shin, R. B. Ambade, J. H. Bang, H. W. Kim and T. H. Han, *ACS Appl. Mater. Interfaces*, 2020, **12**, 10434–10442.
232 Z. Liu, H. Lv, Y. Zhang, J. W. He, L. Han, S. Li, L. Yang and Y. Xu, *ACS Sens.*, 2024, **9**, 3641–3651.
233 X. Tian, X. Cui, B. Yao, S. Wang, H. Li, T. Chen, X. Xiao and Y. Wang, *Sens. Actuators, B*, 2023, **395**, 134449.
234 C. Park, J. W. Baek, E. Shin and I.-D. Kim, *ACS Nanosci. Au*, 2023, **3**, 353–374.
235 A. Sharma, S. B. Eadi, H. Noothalapati, M. Otyepka, H.-D. Lee and K. Jayaramulu, *Chem. Soc. Rev.*, 2024, **53**, 2530–2577.
236 M. Jeon, J.-S. Lee, M. Kim, J.-W. Seo, H. Kim, H. R. Moon, S.-J. Choi and J. Kim, *ACS Appl. Mater. Interfaces*, 2024, **16**, 62382–62391.
237 J.-H. Kim, A. Mirzaei, I. Sakaguchi, S. Hishita, T. Ohsawa, T. T. Suzuki, S. Sub Kim and N. Saito, *Appl. Surf. Sci.*, 2023, **641**, 158478.
238 W. Quan, J. Shi, H. Luo, C. Fan, W. Lv, X. Chen, M. Zeng, J. Yang, N. Hu, Y. Su, H. Wei and Z. Yang, *ACS Sens.*, 2023, **8**, 103–113.
239 W.-T. Koo, J.-S. Jang and I.-D. Kim, *Chem*, 2019, **5**, 1938–1963.
240 Z. Yuan, M. Bariya, H. M. Fahad, J. Wu, R. Han, N. Gupta and A. Javey, *Adv. Mater.*, 2020, **32**, 1908385.
241 N. Goel, Utkarsha, A. Kushwaha, M. Kwoka, R. Kumar and M. Kumar, *J. Mater. Chem. A*, 2024, **12**, 5642–5667.
242 Z. Liang, M. Wang, X. Zhang, Z. Li, K. Du, J. Yang, S.-Y. Lei, G. Qiao, J. Z. Ou and G. Liu, *ACS Nano*, 2024, **18**, 3669–3680.
243 M.-S. Yao, J.-W. Xiu, Q.-Q. Huang, W.-H. Li, W.-W. Wu, A.-Q. Wu, L.-A. Cao, W.-H. Deng, G.-E. Wang and G. Xu, *Angew. Chem., Int. Ed.*, 2019, **58**, 14915–14919.
244 S. S. Gaikwad, A. S. Khune, N. N. Ingle and M. D. Shirsat, *Sens. Actuators, A*, 2024, **377**, 115665.
245 B. Bhangare, K. R. Sinju, N. S. Ramgir, S. Gosavi and A. K. Debnath, *Mater. Sci. Semicond. Process.*, 2022, **147**, 106706.
246 C. Tang, W. Jin, X. Xiao, X. Qi, Y. Ma and L. Ma, *Sens. Actuators, B*, 2025, **424**, 136889.
247 J. Li, H. Zhao, Y. Wang, R. Zhang, C. Zou and Y. Zhou, *Anal. Chem.*, 2022, **94**, 16160–16170.
248 S. Kanaparthi and S. G. Singh, *ACS Sustainable Chem. Eng.*, 2021, **9**, 14735–14743.
249 P. Patel, A. Pandey, V. Bonu, K. K. Madapu, O. P. Khatri and H. C. Barshilia, *Phys. B*, 2025, **705**, 417087.
250 S. Gaur, S. Singh, A. Bhatia, V. Bhutani, M. Verma, H. Haick, V. Pareek and R. Gupta, *Adv. Funct. Mater.*, 2025, **35**, 2417729.
251 D. Han, X. Han, X. Zhang, W. Wang, D. Li, H. Li and S. Sang, *Sens. Actuators, B*, 2022, **367**, 132038.
252 W. Ding, J. Yu, F. Tsow, L. R. Jaishi, B. S. Lamsal, R. Kittelson, S. Ahmed, P. Kharel, Y. Zhou and X. Xian, *npj 2D Mater. Appl.*, 2024, **8**, 18.
253 B. Huang, X. Tong, X. Zhang, Q. Feng, M. N. Rumyantseva, J. Prakash and X. Li, *Chemosensors*, 2023, **11**, 258.
254 J. Ding, Q. Wang, X. Liu, S. Li and H. Li, *J. Hazard. Mater.*, 2024, **480**, 136261.
255 W. Y. Chen, X. Jiang, S.-N. Lai, D. Peroulis and L. Stanciu, *Nat. Commun.*, 2020, **11**, 1302.
256 P. Chen, X. Su, C. Wang, G. Zhang, T. Zhang, G. Xu and L. Chen, *Angew. Chem., Int. Ed.*, 2023, **135**, e202306224.
257 D. Pandey, T. Samarth, V. K. Verma, C. Patel, L. Ponvijayakanthan, N. K. Jaiswal, S. Mukherjee and A. Raghuvanshi, *J. Mater. Chem. A*, 2025, **13**, 11416–11424.
258 P. Salvo, B. Melai, N. Calisi, C. Paoletti, F. Bellagambi, A. Kirchhain, M. G. Trivella, R. Fuoco and F. Di Francesco, *Sens. Actuators, B*, 2018, **256**, 976–991.
259 S. Ghosh, A. Pannone, D. Sen, A. Wali, H. Ravichandran and S. Das, *Nat. Commun.*, 2023, **14**, 6021.
260 Y. Yu, P. C. Joshi, J. Wu and A. Hu, *ACS Appl. Mater. Interfaces*, 2018, **10**, 34005–34012.
261 H. Zhi, X. Zhang, F. Wang and L. Feng, *ACS Appl. Mater. Interfaces*, 2022, **14**, 52422–52429.
262 S. Veeralingam and S. Badhulika, *Nanoscale*, 2020, **12**, 15336–15347.
263 J. Liu, N. Zhang, J. Li, M. Li, G. Wang, W. Wang, Y. Fan, S. Jiang, G. Chen, Y. Zhang, X. Sun and Y. Liu, *Food Chem.*, 2022, **397**, 133838.
264 M. D. Wagh, S. K. Sahoo and S. Goel, *Sens. Actuators, A*, 2022, **333**, 113301.
265 C. Gao, F. Liu, C. Gu, R. Singh, B. Zhang and S. Kumar, *IEEE Sens. J.*, 2024, **24**, 22336–22343.
266 J. Yi, X. Chen, Q. Weng, Y. Zhou, Z. Han, J. Chen and C. Li, *Electrochem. Commun.*, 2020, **118**, 106796.
267 T.-H. Chang, Y. Tian, C. Li, X. Gu, K. Li, H. Yang, P. Sanghani, C. M. Lim, H. Ren and P.-Y. Chen, *ACS Appl. Mater. Interfaces*, 2019, **11**, 10226–10236.
268 Y. He, X. Xu, S. Xiao, J. Wu, P. Zhou, L. Chen and H. Liu, *ACS Sens.*, 2024, **9**, 2275–2293.
269 J. Wang, Y. Luo, X. J. Loh and X. Chen, *Matter*, 2024, **7**, 2368–2381.

270 S. Duan, Q. Shi and J. Wu, *Adv. Intell. Syst.*, 2022, **4**, 2200213.
271 S. Deng, Y. Li, S. Li, S. Yuan, H. Zhu, J. Bai, J. Xu, L. Peng, T. Li and T. Zhang, *The Innovation*, 2024, **5**, 100596.
272 M. Saeidi-Javash, Y. Du, M. Zeng, B. C. Wyatt, B. Zhang, N. Kempf, B. Anasori and Y. Zhang, *ACS Appl. Electron. Mater.*, 2021, **3**, 2341–2348.
273 J. Zhang, L. Qin, R. Ma, M. B. Bakarić and B. Tobolková, *ACS Appl. Mater. Interfaces*, 2024, **16**, 58848–58863.
274 K.-Y. Chen, Y.-T. Xu, Y. Zhao, J.-K. Li, X.-P. Wang and L.-T. Qu, *Nano Mater. Sci.*, 2023, **5**, 247–264.
275 J. Qu, G. Cui, Z. Li, S. Fang, X. Zhang, A. Liu, M. Han, H. Liu, X. Wang and X. Wang, *Adv. Funct. Mater.*, 2024, **34**, 2401311.
276 T. Yuan, R. Yin, C. Li, Z. Fan and L. Pan, *Chem. Eng. J.*, 2024, **487**, 150396.
277 Y. Zhou, S. Huang, Z. Xu, P. Wang, X. Wu and D. Zhang, *IEEE Trans. Cognit. Dev. Syst.*, 2022, **14**, 799–818.
278 L. Li, G. Jia, W. Huang, J. Zhou, C. Li, J. Han, Y. Zhang and X. Zhou, *Sens. Actuators, A*, 2023, **351**, 114149.
279 P. Zhou, J. Lin, W. Zhang, Z. Luo and L. Chen, *Nano Res.*, 2022, **15**, 5376–5383.
280 A. Hussnain, S. Kulkarni and K. A. Khan, *Sci. Rep.*, 2024, **14**, 20244.
281 H. Wang, Z. Zhao, P. Liu, Y. Pan and X. Guo, *ACS Appl. Mater. Interfaces*, 2022, **14**, 41283–41295.
282 L. Xu, H. Zheng, F. Xue, Q. Ji, C. Qiu, Q. Yan, R. Ding, X. Zhao, Y. Hu, Q. Peng and X. He, *Chem. Eng. J.*, 2023, **463**, 142392.
283 T. Zhao, H. Liu, L. Yuan, X. Tian, X. Xue, T. Li, L. Yin and J. Zhang, *Adv. Mater. Interfaces*, 2022, **9**, 2101948.
284 J. Zhou, H. Chen, Z. Wu, P. Zhou, M. You, C. Zheng, Q. Guo, Z. Li and M. Weng, *Nano Energy*, 2025, **134**, 110552.
285 P. Li, N. Su, Z. Wang and J. Qiu, *ACS Nano*, 2021, **15**, 16811–16818.
286 Y. Wang, Z. Luo, Y. Qian, W. Zhang and L. Chen, *Chem. Eng. J.*, 2023, **454**, 140513.
287 D. Gao, M.-F. Lin, J. Xiong, S. Li, S. N. Lou, Y. Liu, J.-H. Ciou, X. Zhou and P. S. Lee, *Nanoscale Horiz.*, 2020, **5**, 730–738.
288 J. Liu, S. He, Z. Liu, X. Wu, J. Liu and W. Shao, *Sens. Actuators, B*, 2023, **393**, 134217.
289 D.-D. Han, Y.-Q. Liu, J.-N. Ma, J.-W. Mao, Z.-D. Chen, Y.-L. Zhang and H.-B. Sun, *Adv. Mater. Technol.*, 2018, **3**, 1800258.
290 H. Riazi, G. Taghizadeh and M. Soroush, *ACS Omega*, 2021, **6**, 11103–11112.
291 Y. Hu, K. Qi, L. Chang, J. Liu, L. Yang, M. Huang, G. Wu, P. Lu, W. Chen and Y. Wu, *J. Mater. Chem. C*, 2019, **7**, 6879–6888.
292 H. Cheng, F. Zhao, J. Xue, G. Shi, L. Jiang and L. Qu, *ACS Nano*, 2016, **10**, 9529–9535.
293 L. Chen, M. Weng, P. Zhou, F. Huang, C. Liu, S. Fan and W. Zhang, *Adv. Funct. Mater.*, 2019, **29**, 1806057.
294 A. Shayesteh Zeraati, S. A. Mirkhani, P. Sun, M. Naguib, P. V. Braun and U. Sundararaj, *Nanoscale*, 2021, **13**, 3572–3580.
295 H. An, T. Habib, S. Shah, H. Gao, A. Patel, I. Echols, X. Zhao, M. Radovic, M. J. Green and J. L. Lutkenhaus, *ACS Appl. Nano Mater.*, 2019, **2**, 948–955.
296 R. Li, L. Zhang, L. Shi and P. Wang, *ACS Nano*, 2017, **11**, 3752–3759.
297 H. Lin, X. Wang, L. Yu, Y. Chen and J. Shi, *Nano Lett.*, 2017, **17**, 384–391.
298 T. Sun, B. Feng, J. Huo, Y. Xiao, W. Wang, J. Peng, Z. Li, C. Du, W. Wang and G. Zou, *Nano-Micro Lett.*, 2024, **16**, 14.
299 F. Zhang, C. Li, Z. Li, L. Dong and J. Zhao, *Microsyst. Nanoeng.*, 2023, **9**, 16.
300 G. Lee, J. H. Baek, F. Ren, S. J. Pearton, G. H. Lee and J. Kim, *Small*, 2021, **17**, 2100640.
301 C. Zhang, H. Zhou, S. Chen, G. Zhang, Z. G. Yu, D. Chi, Y.-W. Zhang and K.-W. Ang, *Crit. Rev. Solid State Mater. Sci.*, 2022, **47**, 665–690.
302 T. F. Schranghamer, A. Oberoi and S. Das, *Nat. Commun.*, 2020, **11**, 5474.
303 J. Shen, B. Zhou, F. Wang, Q. Wan, X. Shan, C. Li, X. Lin and K. Zhang, *Nanotechnology*, 2020, **31**, 265202.
304 Y. Wang, H. Liu, P. Liu, W. Lu, J. Cui, X. Chen and M. Lu, *J. Alloys Compd.*, 2022, **909**, 164775.
305 S. Seo, J.-J. Lee, H.-J. Lee, H. W. Lee, S. Oh, J. J. Lee, K. Heo and J.-H. Park, *ACS Appl. Electron. Mater.*, 2020, **2**, 371–388.
306 X. Zhao, J. Xuan, Q. Li, F. Gao, X. Xun, Q. Liao and Y. Zhang, *Adv. Mater.*, 2023, **35**, 2207437.
307 J. Klimaszewski, Ł. Gruszka and J. Możaryn, *Cham*, 2022, 115–121.
308 J. Klimaszewski and P. Białorucki, *Cham*, 2023, 242–249.
309 J. O. D. Williams, R. C. Harris and G. A. Solan, *Cham*, 2021, 583–595.
310 H. Zhang, L. Lin, N. Hu, D. Yin, W. Zhu, S. Chen, S. Zhu, W. Yu and Y. Tian, *Carbon*, 2022, **189**, 430–442.
311 C. Choi, M. K. Choi, S. Liu, M. Kim, O. K. Park, C. Im, J. Kim, X. Qin, G. J. Lee, K. W. Cho, M. Kim, E. Joh, J. Lee, D. Son, S.-H. Kwon, N. L. Jeon, Y. M. Song, N. Lu and D.-H. Kim, *Nat. Commun.*, 2017, **8**, 1664.
312 H. Wang, D.-R. Chen, Y.-C. Lin, P.-H. Lin, J.-T. Chang, J. Muthu, M. Hofmann and Y.-P. Hsieh, *ACS Nano*, 2024, **18**, 19828–19835.
313 M. Sitti, *Extreme Mech. Lett.*, 2021, **46**, 101340.
314 H. Oh, G.-C. Yi, M. Yip and S. A. Dayeh, *Sci. Adv.*, 2020, **6**, eabd7795.